NASA TECHNICAL
MEMORANDUM
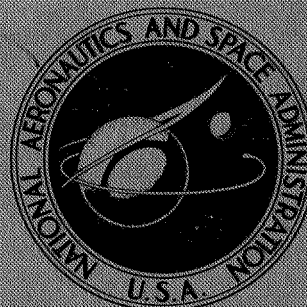
NASA TM X-960

NASA TM X-960

N67-31933
(ACCESSION NUMBER)

45
(PAGES)

TMX-960
(NASA CR OR TMX OR AD NUMBER)

(THRU)

(CODE)

02
(CATEGORY)

FACILITY FORM 602

AERODYNAMIC CHARACTERISTICS OF
A TAILLESS FIXED-WING SUPERSONIC
TRANSPORT CONFIGURATION
AT MACH NUMBER 2.20 (U)

by Gerald V. Foster and William A. Corlett

Langley Research Center,

Langley Station, Hampton, Va.

NATIONAL AERONAUTICS AND SPACE ADMINISTRATION • WASHINGTON, D. C. • MAY 1964

AERODYNAMIC CHARACTERISTICS OF A

TAILLESS FIXED-WING SUPERSONIC TRANSPORT CONFIGURATION

AT MACH NUMBER 2.20

By Gerald V. Foster and William A. Corlett

Langley Research Center
Langley Station, Hampton, Va.

NATIONAL AERONAUTICS **AND** SPACE ADMINISTRATION

AERODYNAMIC CHARACTERISTICS OF A

TAILLESS FIXED-WING SUPERSONIC TRANSPORT CONFIGURATION

AT MACH NUMBER 2.20*

By Gerald V. Foster and William A. Corlett
Langley Research Center

SUMMARY

13883

An investigation has been conducted in the Langley 4- by 4-foot supersonic pressure tunnel at a Mach number of 2.20 to determine the longitudinal and lateral aerodynamic characteristics of a model of a tailless fixed-wing supersonic transport configuration. The model was investigated with three different wing planforms, a trapezoid, a delta, and a modified delta having an ogee-shaped leading edge, with and without camber and twist.

The results indicate that the model was longitudinally stable about the selected center-of-gravity locations with each of the test wings. The cambered and twisted trapezoid-wing configuration had the highest maximum untrimmed lift-drag ratio (6.45). Trim control by means of the elevons was relatively low and significantly lowered the maximum lift-drag ratio of the flat-wing (zero camber) configurations. The trim penalty was diminished by the positive pitching moment provided by camber and twist. The flat-wing configurations and the cambered and twisted delta- and trapezoid-wing configurations had about the same directional stability and were stable to an angle of attack of about 12°. The cambered and twisted ogee-wing configuration had somewhat lower values of the directional stability parameter through the test angle-of-attack range.

INTRODUCTION

The National Aeronautics and Space Administration is currently placing considerable emphasis on configuration studies applicable to a supersonic transport aircraft. These studies have been performed on both variable-sweep and fixed-wing aircraft models at speeds from low subsonic Mach numbers to Mach numbers in excess of 3. Results of some of these studies may be found in references 1 to 6. The fixed-wing configurations studied thus far have included the highly swept arrow-wing type (ref. 5) and the delta-wing canard type (ref. 6). As a continuation of the study of fixed-wing configurations, a tailless delta-wing type has been investigated and the results obtained are presented herein.

---

*Title, Unclassified.

The test configuration consisted of a low-wing—body—vertical-tail arrangement. Three wing planforms were investigated including a delta, a trapezoid, and a modified delta with an ogee-shaped leading edge. In addition, each wing planform was tested with and without camber and twist.

The investigation was performed in the Langley 4- by 4-foot supersonic pressure tunnel at a Mach number of 2.20 and a Reynolds number of 3.0×10^6 per foot. The angle-of-attack range varied from about $-4°$ to $12°$, and the angle-of-sideslip range varied from about $-4°$ to $6°$.

SYMBOLS

The sideslip data are referred to the body-axis system and the pitch data are referred to the stability-axis system. The moment reference for all configurations is located on the model reference line at a point 59.4 percent body length behind the nose. (See fig. 1.)

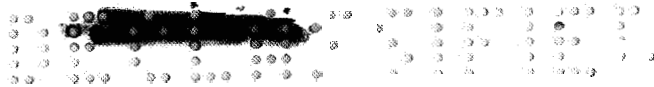|	
b	span of wing, 19.25 in.
C_D	drag coefficient, $\dfrac{\text{Drag}}{qS}$
$C_{D,B}$	nacelle base drag coefficient
$C_{D,b}$	balance chamber drag coefficient
$C_{D,i}$	nacelle internal drag coefficient
C_L	lift coefficient, $\dfrac{\text{Lift}}{qS}$
C_l	rolling-moment coefficient, $\dfrac{\text{Rolling moment}}{qSb}$
C_{l_β}	rolling-moment parameter, $\dfrac{\Delta C_l}{\Delta \beta}$, per deg
C_m	pitching-moment coefficient, $\dfrac{\text{Pitching moment}}{qS\bar{c}}$
C_n	yawing-moment coefficient, $\dfrac{\text{Yawing moment}}{qSb}$
C_{n_β}	yawing-moment parameter, $\dfrac{\Delta C_n}{\Delta \beta}$, per deg

2

C_p · pressure coefficient

C_Y side-force coefficient, $\dfrac{\text{Side force}}{qS}$

C_{Y_β} side-force parameter, $\dfrac{\Delta C_Y}{\Delta \beta}$, per deg

c local chord, in.

$\bar{c}$ reference chord of wing, 12.00 in.

L/D lift-drag ratio

l overall length of wing measured in streamwise direction, in.

M Mach number

q free-stream dynamic pressure, lb/sq ft

R Reynolds number

S area of wing including body intercept, 1.6665 ft

x longitudinal distance measured from wing apex

Y lateral distance measured normal to plane of symmetry, in.

z local camber ordinate measured normal to chord, in.

a angle of attack measured with respect to body reference line, deg

β angle of sideslip, deg

δ_e elevon deflection angle, deg

Model components:

B body

E engine nacelle

V vertical tail

W wing

Subscript:

max   maximum

Model

A drawing of the model with dimensional details is presented as figure **1**.

The wing planforms used for these tests were a delta, a trapezoid, and a modified delta with an ogee-shaped leading edge. The latter planform will henceforth be referred to as the ogee wing. Figure 2 shows a comparison of the planforms of the three wings, and photographs of the model with the ogee wing are presented as figure *3*. Each wing had circular-arc airfoil sections with a streamwise thickness-chord ratio of 0.03 at the roots which varied to 0.02 at the tip. The aspect ratio of the wings was 1.55. Each wing planform was tested with zero camber and a twist and camber designed for a lift coefficient of'O.l. The wings with zero camber will henceforth be referred to as flat wings or $C_{L,design} = 0$.

The theoretical pressure distribution for each planform may be expressed as follows:

For the ogee 'planform,

$$C_p = \pm 1.075 \frac{C_{L,design}}{2}\left[1.5 + 1.45959\left(\frac{y}{b/2}\right) - 1.5\left(\frac{x}{l}\right)\right]$$

for the delta planform,

$$C_p = \pm\frac{C_{L,design}}{2}\left[1.5 + 1.38171\left(\frac{y}{b/2}\right) - 1.5\left(\frac{x}{l}\right)\right]$$

and for the trapezoid planform,

$$C_p = \pm\frac{C_{L,design}}{2}\left[1.5 + 1.335\left(\frac{y}{b/2}\right) - 1.5\left(\frac{x}{l}\right)\right]$$

Mean camber ordinates and spanwise variation of twist determined for these planforms are presented in figure 4. The ogee wing was modified to provide additional leading-edge camber over the outer 35 percent of the wing semispan. This camber modification amounted to a maximum deflection of the leading edge of 0.1 inch.

The flat wings were equipped with plain flap-type, trailing-edge elevons located both inboard and outboard of the nacelles. The spanwise location of the

nacelles on the flat wings are shown in figure 1. With the warped wings the "nacelles were moved inboard so that the nacelle center line was 3.65 inches from the model center line.

The vertical tail had 3-percent biconvex airfoil sections and was constructed as an integral part of the fuselage; therefore, tail-off tests were not a part of the present test sequence.

Tunnel and Measurements

The tests were performed in the Langley 4- by 4-foot supersonic pressure tunnel which is a continuous-flow, variable pressure tunnel. Mach numbers from 1.4 to 2.2 may be obtained for this facility by manually changing the throat size and contour leading to the test section.

Forces and moments on the model were measured by means of a six-component, electrical strain-gage balance mounted within the fuselage. Nacelle base pressures and balance cavity pressure were measured by means of single static orifices in the balance cavity and on the nacelle base.

TESTS, CORRECTIONS, AND ACCURACY

The test conditions were as follows:

Machnumber.. . . . . 2.20
Stagnation temperature, ^{o}F 100
Stagnation pressure, lb/sq ft 1708
Test Reynolds number per foot . . . . 3.0 x 10^6

The stagnation dewpoint was maintained sufficiently low (-25° or less) to prevent condensation from occurring in the test section. Tests were made through an angle-of-attack range from approximately -4° to 12° at $\beta = 0^o$ and $\beta = 4^o$ and through a range of sideslip angles from approximately -4° to 6° at angles of attack of approximately 0° and 8°. The angles of attack and sideslip have been corrected for deflection of the balance and sting due to aerodynamic load. The drag forces were adjusted to a nacelle base pressure and a balance cavity pressure equal to free-stream static pressure. The variations of nacelle base and balance cavity-drag coefficients with angle of attack are presented in figure 5.

Since the nacelle ducts had no change in internal shape or cross-sectional area, the internal drag coefficient was computed using the method described in reference 7. The variation of internal drag coefficient with angle of attack is also presented in figure 5.

In an effort to insure a turbulent boundary layer, 1/16-inch-wide transition strips of No. 60 carborundum grains were applied 3/16 inch behind and normal to the leading edges of the wings and tail and 1 inch behind the body nose.

5

The minimum drag coefficients for the flat trapezoidal wing were measured over a Reynolds number range of 1.3×10^6 to 6.0×10^6 and compared with the theoretical estimate (ref. 7) for turbulent flow (fig. 6). The test Reynolds number of 3.0×10^6 appears to be well above the region of transition from laminar to turbulent flow. At Reynolds numbers above about 4.5×10^6, the possibility of drag due to the carborundum grains is indicated.

Based on pretest calibration and repeatability of the data, the data presented herein are estimated to be accurate within the following limits:

C_L . . . .   ±0.0030

C_D . . . .   ±0.0005

C_m . . . .   ±0.0003

C_Z . . . .   ±0.0001

C_n . . . .   ±0.0002

C_Y . . . .   ±0.0015

M . . . .   ±0.01

α, deg . . . .   ±0.1

β, deg . . . .   ±0.1

RESULTS AND DISCUSSION

Pitch Characteristics

The effect of wing planform on the longitudinal characteristics of the flat-wing configurations is presented in figure 7. All these configurations had relatively linear variation of lift and pitching-moment coefficients with angle of attack, and all the configurations were stable about the center-of-gravity location for these tests. On the basis of the same static margin, all of the configurations produced essentially the same pitching-moment characteristics. The trapezoid-wing configuration provided the highest lift-curve slope whereas the ogee-wing configuration provided the lowest lift-curve slope. The trapezoid-wing configuration also had the highest maximum lift-drag ratio of the three planform configurations even though the ogee-wing configuration had the lowest values of minimum drag coefficient. The maximum lift-drag ratio for the trapezoid-wing configuration with nacelles on was about 5.95 compared with about 5.80 for both the ogee-wing and delta-wing configurations. The nacelles had little or no effect on the lift and stability characteristics of any of the configurations. Although, as expected, they caused an increase in drag coefficient and a decrease in lift-drag ratios.

The effectiveness of the elevons in trimming the flat-wing configurations is shown in figure 8. The results indicate that the maximum elevon deflection investigated ($-10°$) is not sufficient to trim any of the Configurations to the lift coefficient for $(L/D)_{max}$ for the center-of-gravity position used for these tests. Furthermore, if the center-of-gravity position is moved to allow

the configurations to be trimmed to $C_{L(L/D)_{max}}$ with an elevon setting of -10°, the performance penalty due to trimming with the elevons is large (about 0.8 decrement in $(L/D)_{max}$).

The effect of twist and camber on the three wing planform configurations is presented in figure 9. For each planform, the twist and camber reduced the drag due to lift and caused only a slight increase in minimum drag. As a result the maximum values of L/D were increased by about 0.5, leading to an $(L/D)_{max}$ for the trapezoid-wing configuration of 6.45. In addition, twist and camber provided a positive increment in C_m at zero lift for each configuration which would tend to lessen the trimming penalty. The additional camber of the modified ogee wing had little or no effect on the stability or performance characteristics of the configuration (fig. 9(a)).

Sideslip Characteristics

The basic aerodynamic characteristics in sideslip for the flat-trapezoid-wing configuration for angles of attack near 0° and 8° are presented in figure 10 in order to show the linearity of the data since the sideslip parameters C_{n_β}, C_{l_β}, and C_{Y_β} were obtained from incremental results of pitch tests at sideslip angles near 0° and 4°.

Figure 11 shows the effect of wing planform on the sideslip parameters for the configurations with and without twist and camber. There are no large differences in directional stability for the flat-wing configurations and each is stable to an angle of attack near 12°. A positive dihedral effect was obtained with each configuration throughout the test angle-of-attack range. With the wings twisted and cambered, the delta- and trapezoid-wing configurations produced essentially the same degree of directional stability as the flat-wing configuration; however, the cambered ogee-wing configuration showed a marked decrease in directional stability at all test angles of attack (fig. 11(b)). In comparison to the flat-wing values, the C_{l_β} values for the cambered configurations indicated a reduction in the positive dihedral effect throughout the angle-of-attack range. Subsequent tests of the model with the vertical tail removed indicate that the differences in C_{n_β} shown by the cambered ogee wing in comparison to the other wings are inherent in the ogee-wing warp and are not the result of any change in tail contribution.

The effects of various model components on the sideslip characteristics of the cambered wing configurations are presented in figure 12. The effect of the engine nacelles is to increase the side force and, since the nacelles are aft of the moment center, to increase the directional stability. In addition, the presence of the nacelles increased the positive dihedral effect, apparently because of the interference flow fields induced on the underside of the wing. The presence of the wing apparently provides an increase in side force from the tail and an attendant increase in C_{n_β} except for the ogee wing in which case

the stability increase is offset by the decrement inherent in the ogee-wing camber.

Roll Control Characteristics

In order to determine the elevon roll control effectiveness, exploratory tests were performed in which the left outboard elevon on the flat-ogee-wing configurations was deflected -10° and these results are presented in figure 13. These data indicate positive roll effectiveness that decreases slightly with increasing angle of attack. A small favorable yawing moment that occurs at low angles of attack decreases and becomes slightly adverse at the highest angle of attack.

CONCLUSIONS

An investigation has been performed on a fixed-wing supersonic configuration at a Mach number of 2.20. Three wing planforms with and without twist and camber were used on the configuration. The results of these tests lead to the following conclusions:

1. The model was longitudinally stable about the selected center-of-gravity locations with each of the test wings.

2. The cambered and twisted trapezoid-wing configuration had the highest maximum untrimmed lift-drag ratio (6.45) of any of the test configurations.

3. Trim control by means of the elevons was relatively low and significantly lowered the maximum lift-drag ratio of the flat-wing models. The trim penalty was diminished by the positive pitching moment provided by camber and twist.

4. The flat-wing configurations and the cambered and twisted delta- and trapezoid-wing configurations had about the same directional stability and were stable to an angle of attack of about 12°. The cambered and twisted ogee-wing configuration had somewhat lower values of the directional stability parameter through the test angle-of-attack range.

Langley Research Center,
    National Aeronautics and Space Administration,
        Langley Station, Hampton, Va., January 13, 1964.

REFERENCES

1. Staff of the Langley Research Center: The Supersonic Transport - A Technical Summary. NASA TN D-423, 1960.

2. Sleeman, William C., Jr., and Robins, A. Warner: Low-Speed Investigation of the Aerodynamic Characteristics of a Variable-Sweep Supersonic Transport Configuration Having a Blended Wing and Body. NASA TM x-619, 1962.

3. Spearman, M. Leroy, Driver, Cornelius, and Robins, A. Warner: Aerodynamic Characteristics at Mach Numbers of 2.30, 2.96, and 3.50 of a Supersonic Transport Model With a Blended Wing-Body, Variable-Sweep Auxiliary Wing Panels, and Outboard Tail Surfaces. NASA TM x-803, 1963.

4. Driver, Cornelius, Spearman, M. Leroy, and Corlett, William A.: Aerodynamic Characteristics at Mach Numbers From 1.61 to 2.86 of a Supersonic Transport Model With a Blended Wing-Body, Variable-Sweep Auxiliary Wing Panels, Outboard Tail Surfaces, and a Design Mach Number of 2.2. NASA TM x-817, 1963.

5. Whitcomb, Richard T., Patterson, James C., Jr., and Kelly, Thomas C.: An Investigation of the Subsonic, Transonic, and Supersonic Aerodynamic Characteristics of a Proposed Arrow-Wing Transport Airplane Configuration. NASA TM x-800, 1963.

6. Fletcher, LeRoy S.: Static Stability Characteristics of a Delta-Winged Airplane Configuration With Nacelles, a Trapezoidal Canard and a Drooped Tail at Mach Numbers From 0.70 to 3.52. NASA TM x-780, 1963.

7. Sommer, Simon C., and Short, Barbara J.: Free-Flight Measurements of Turbulent-Boundary-Layer Skin Friction in the Presence of Severe Aerodynamic Heating at Mach Numbers From 2.8 to 7.0. NACA TN 3391, 1955.
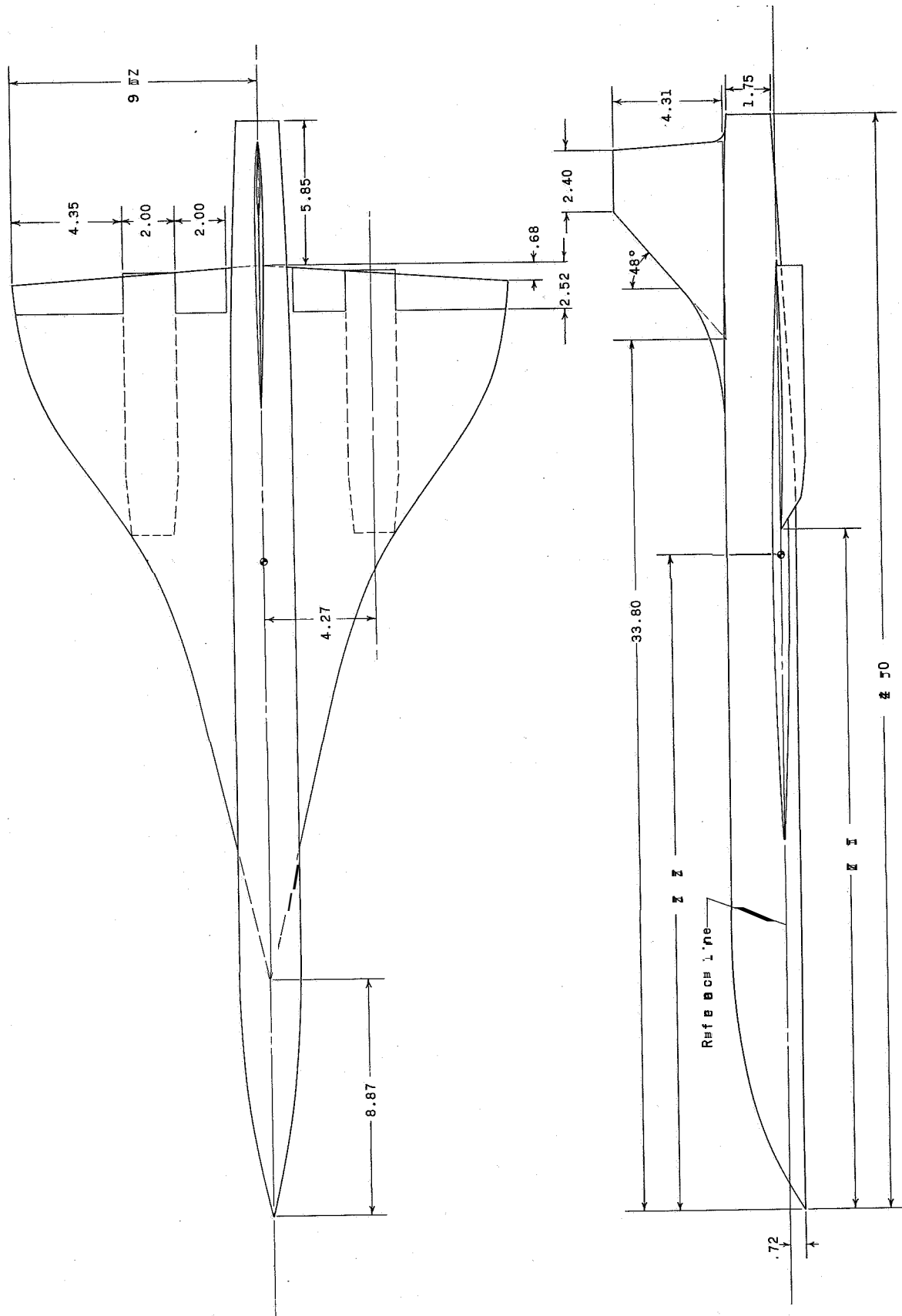
(a) Ogee-wing configuration.

Figure 1.- Details of model. All dimensions are in inches unless otherwise noted.

(b) Delta-wing configuration.
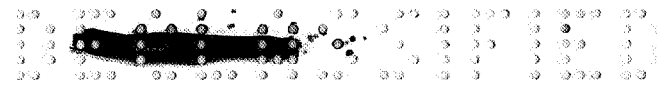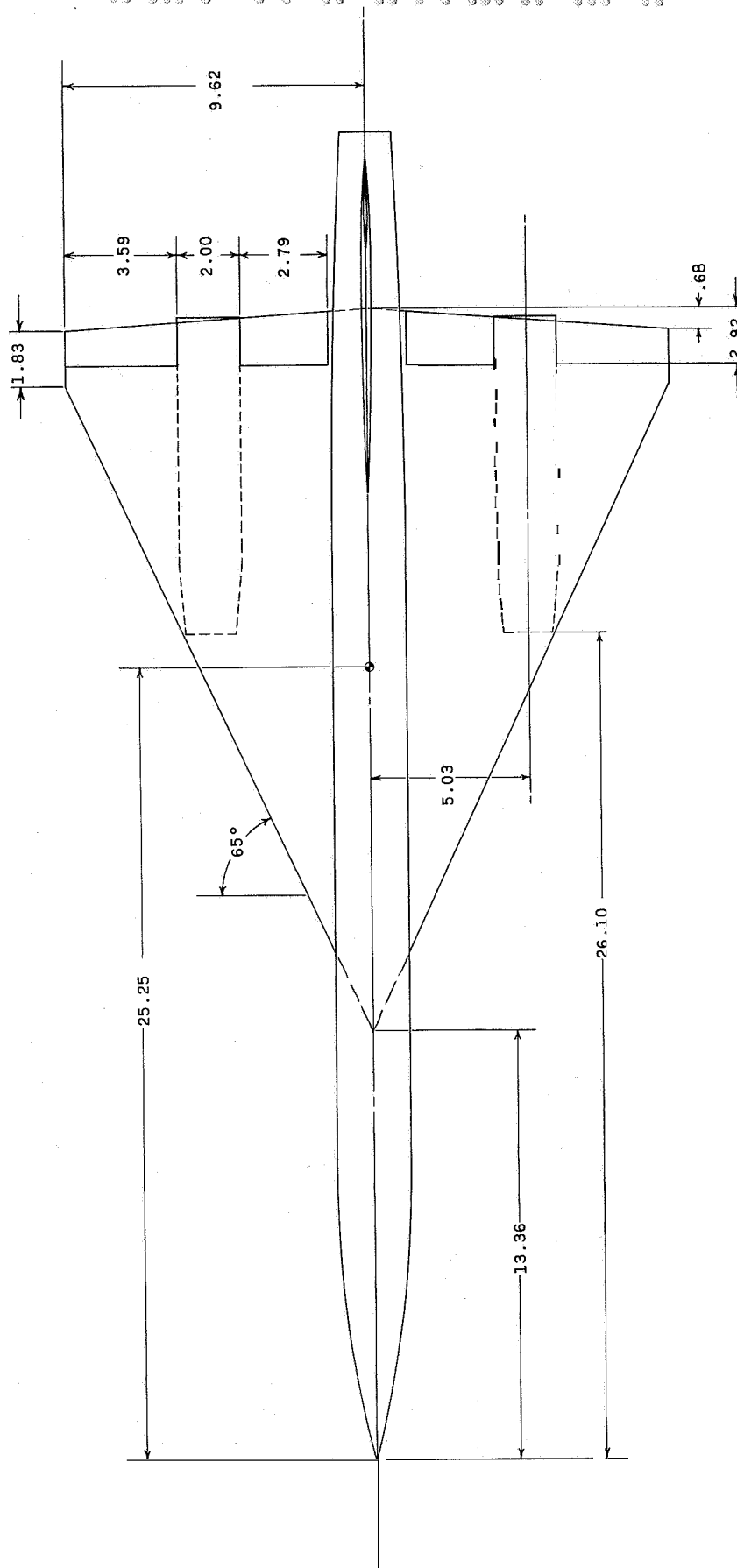
Figure 1.- Continued.

(c) Trapezoid-wing configuration.

Figure 1.- Continued.
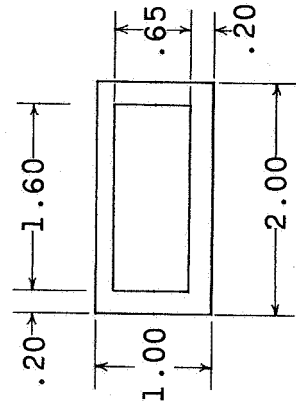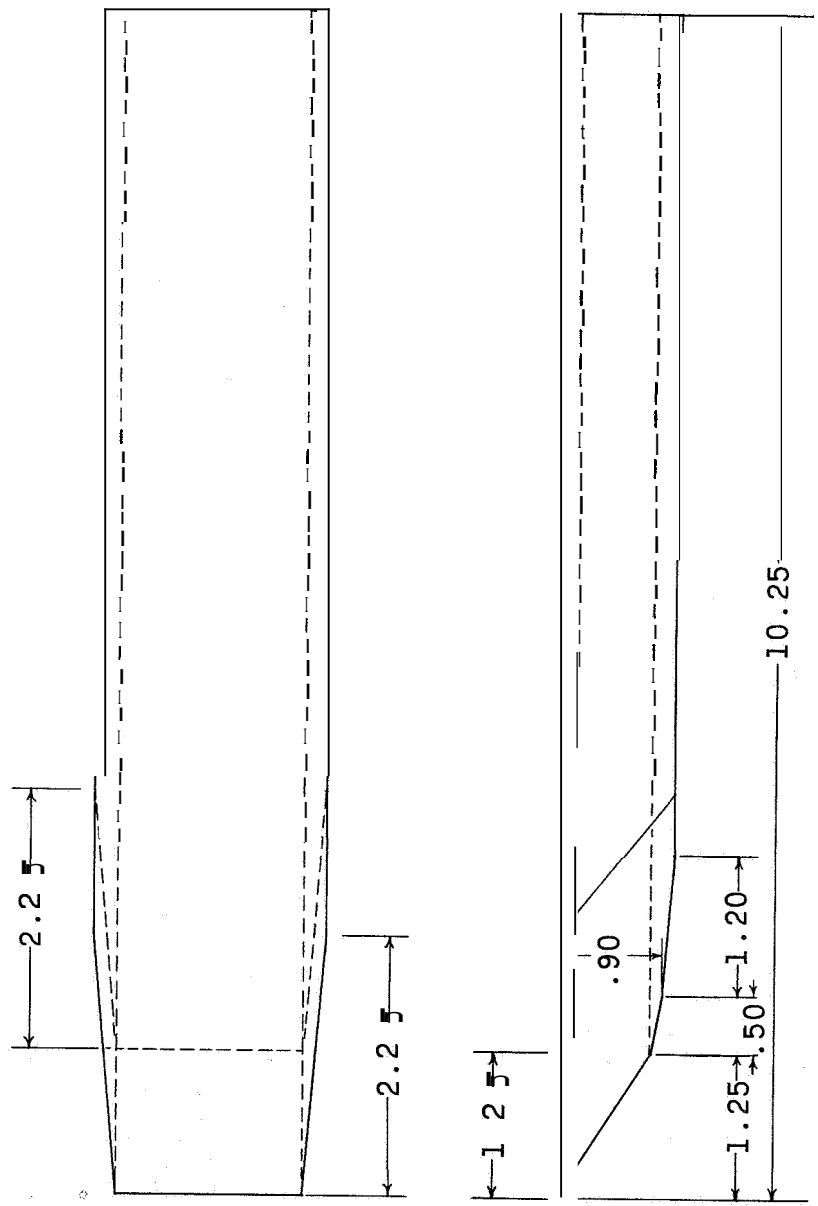
(d) Nacelle.

Figure 1.- Concluded.

13
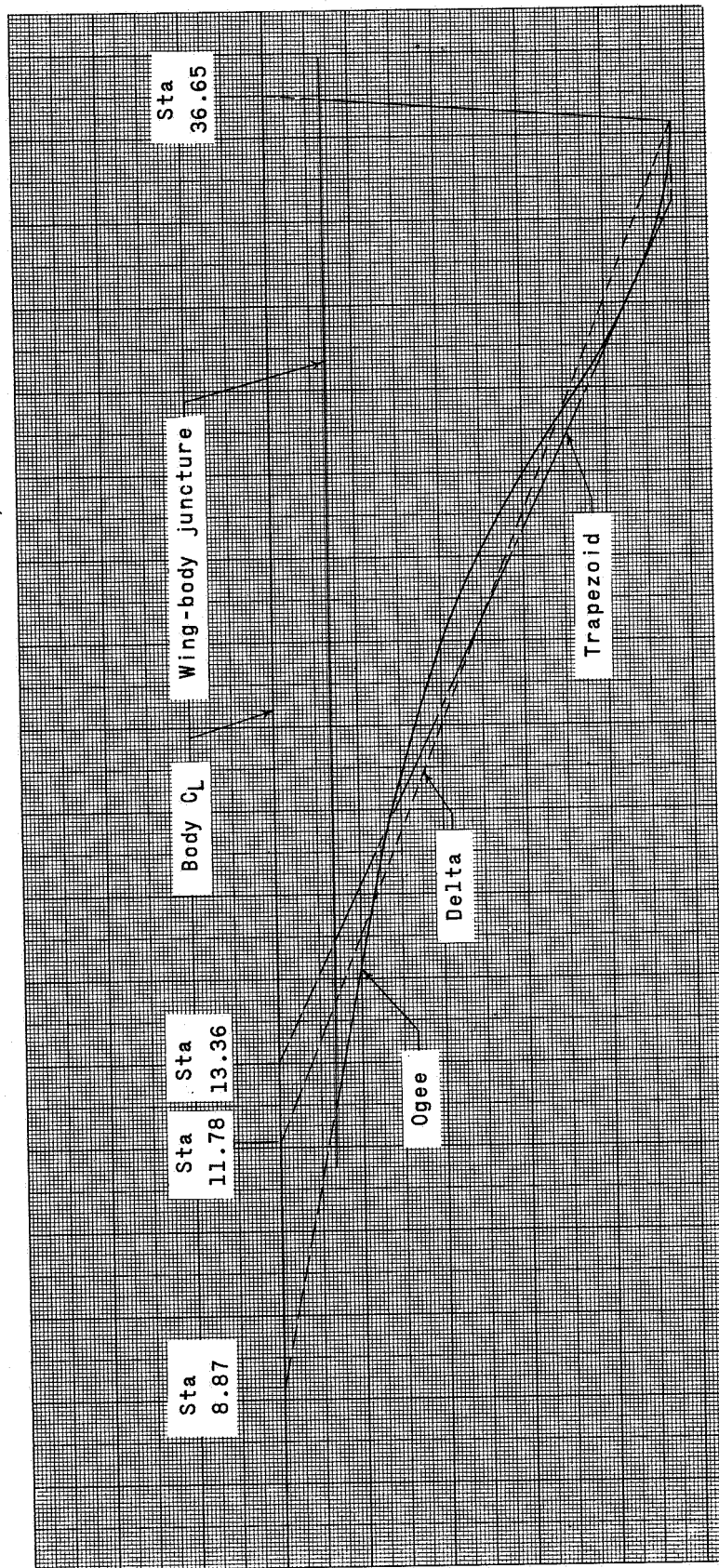
Figure 2.- Comparison of wing planforms.
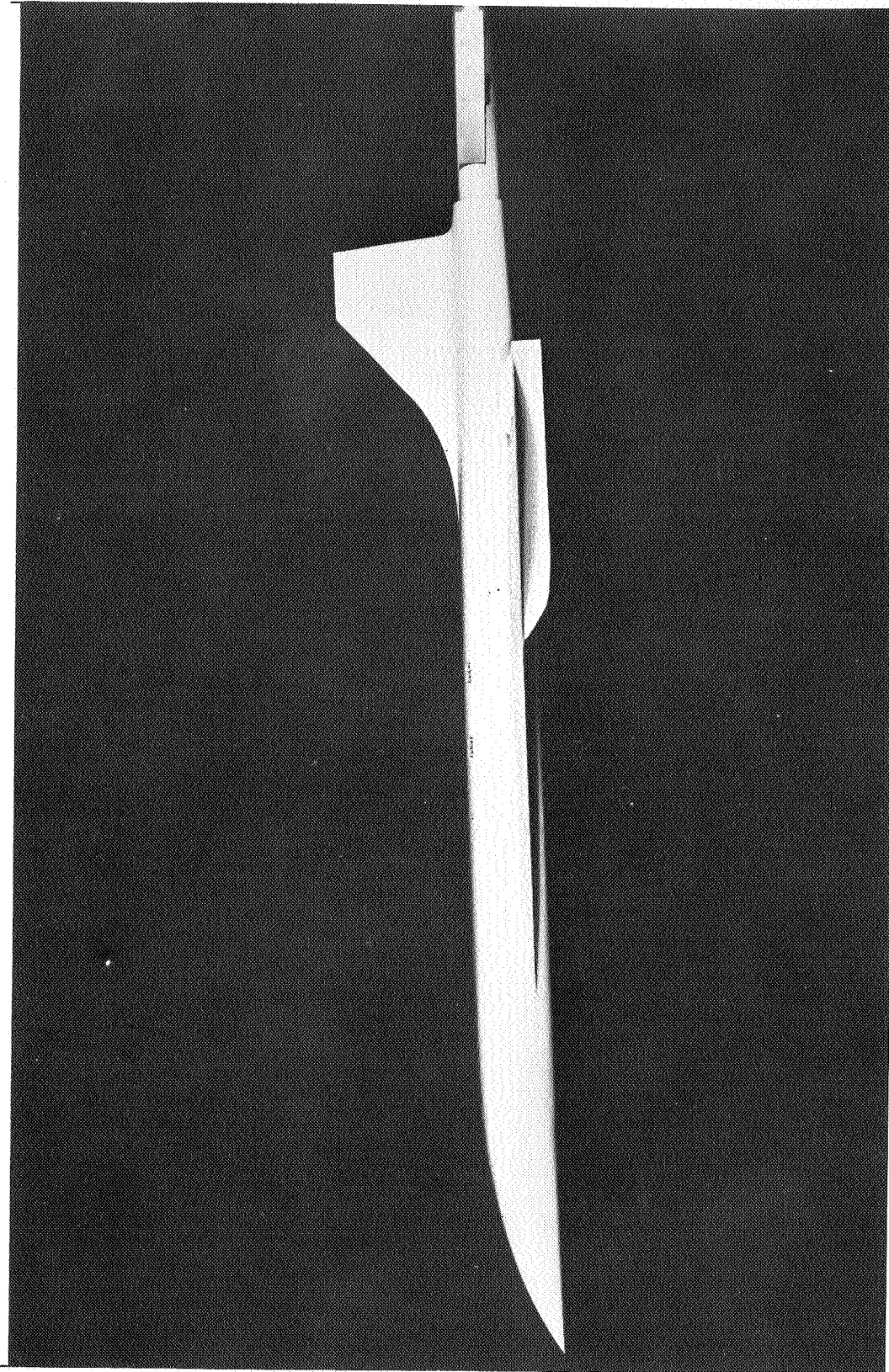
(a) Side view.

Figure 3.- Photographs of model with ogee wing. $C_{L,design} = 0$

L-63-6540
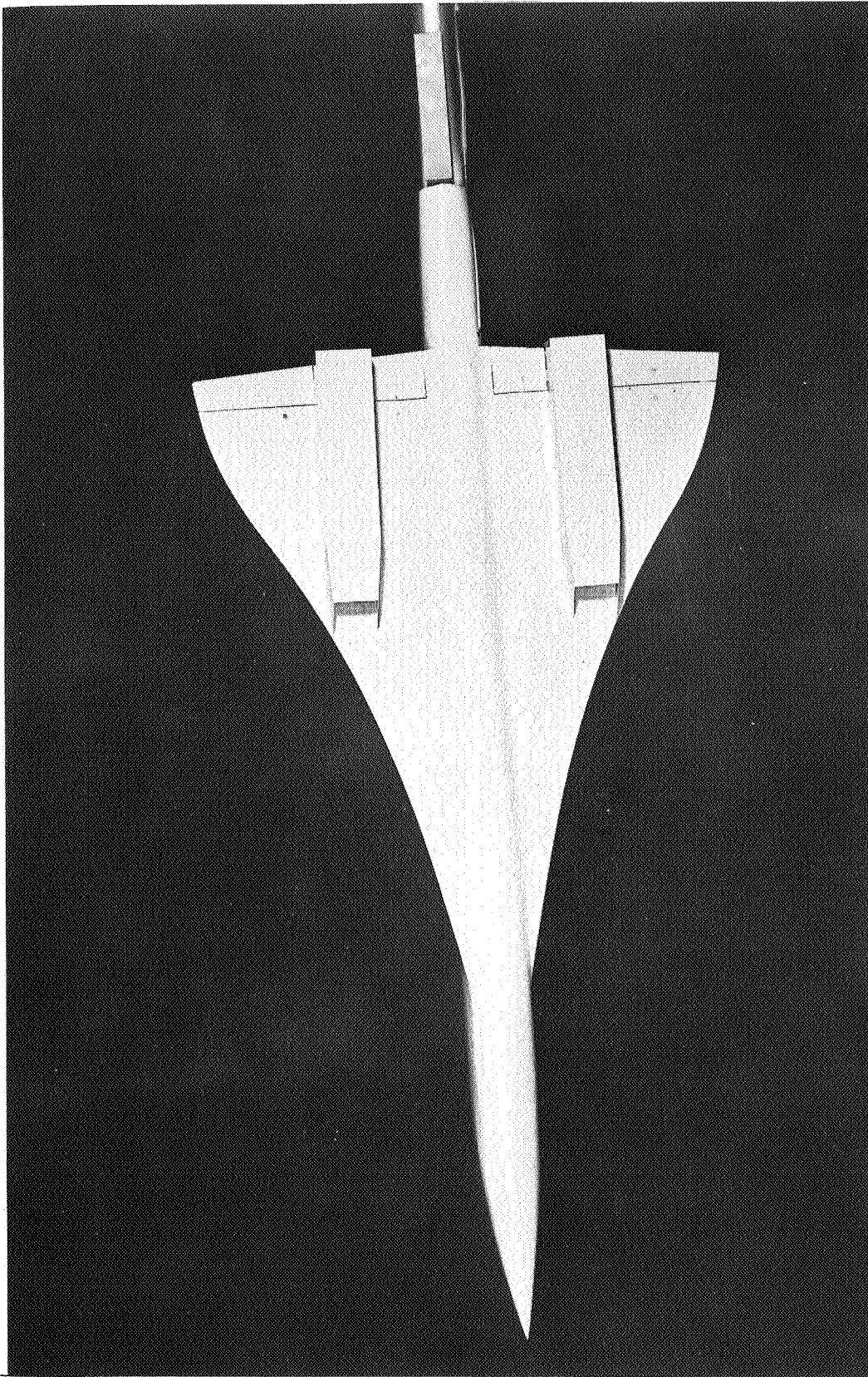
(b) Bottom view.

Figure 3.- Concluded.

L-63-6541
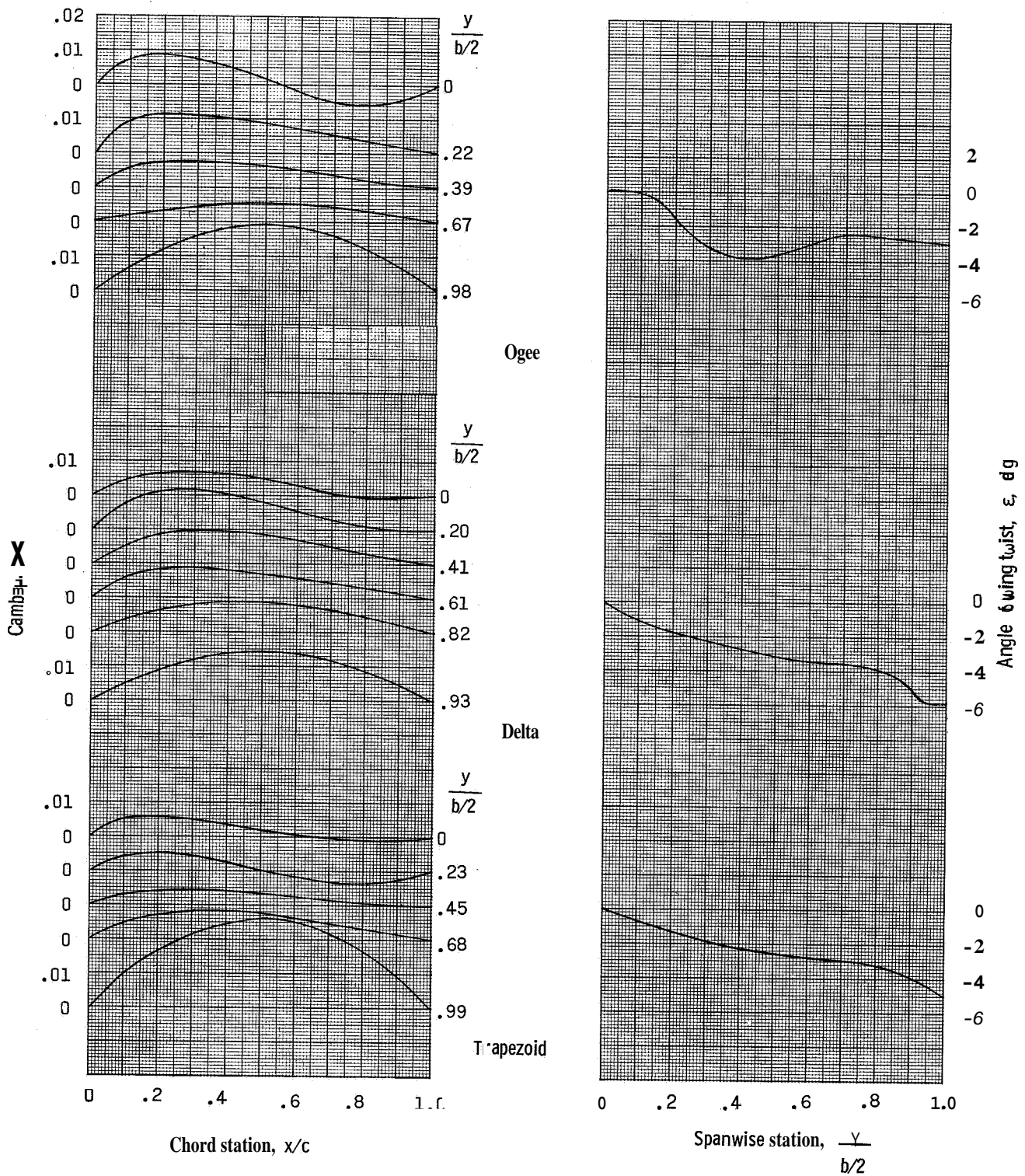
Figure 4.- Variation of camber and twist distribution for ogee-, delta-, and trapezoid-wing configurations.
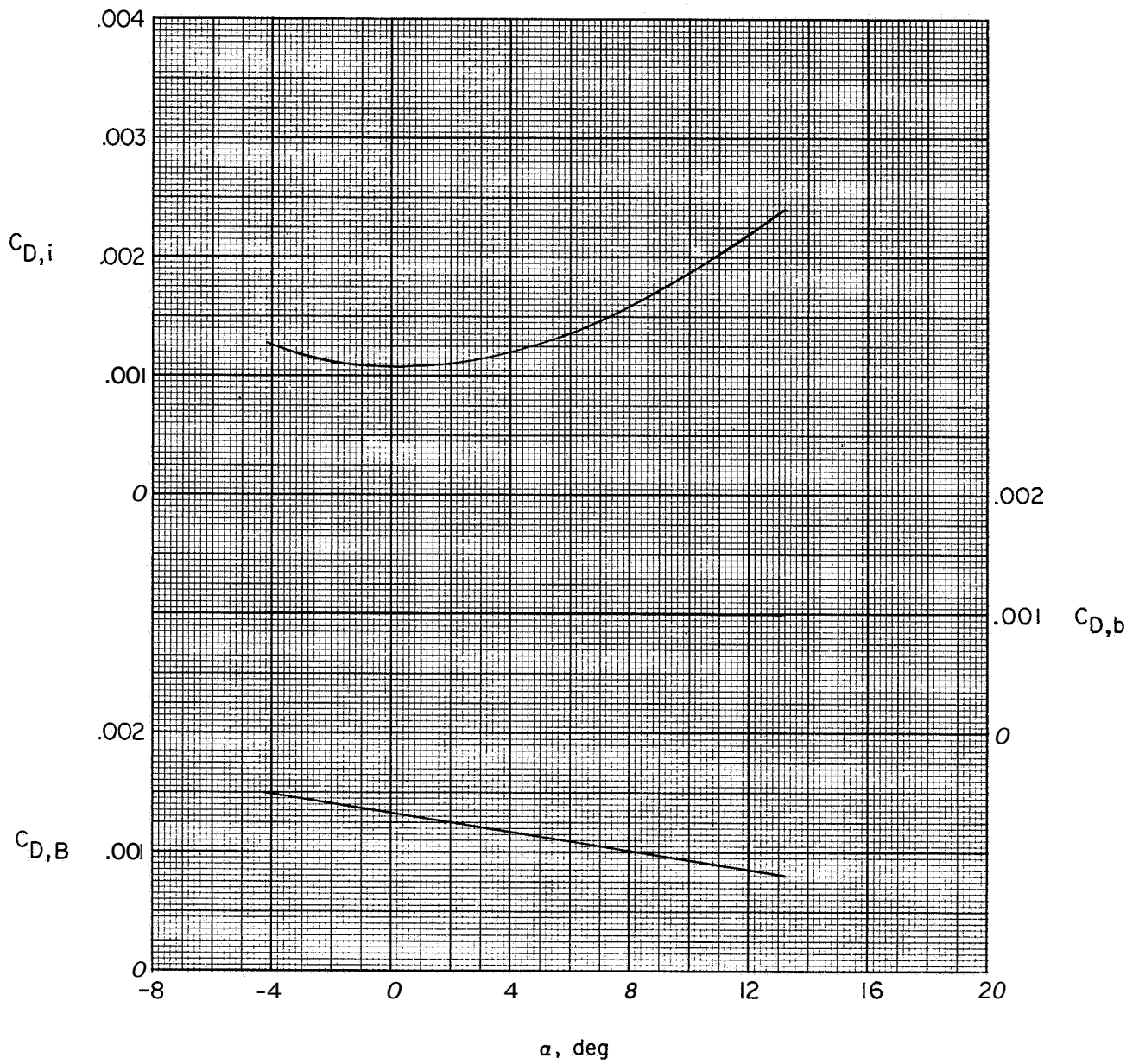
Figure 5.- Variation of balance chamber, nacelle internal, and nacelle base drag coefficients with angle of attack.
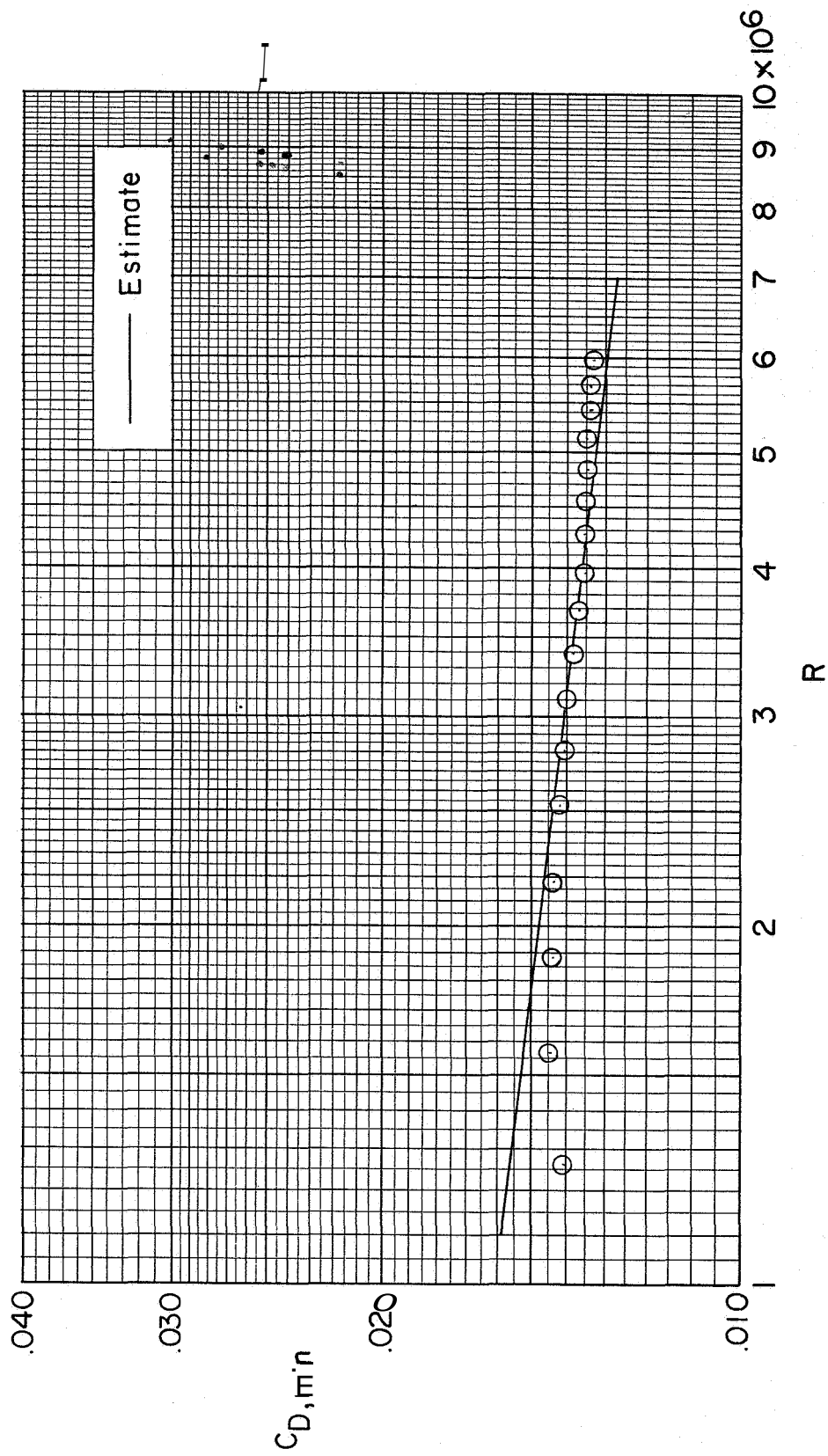
Figure 6.- Variation of minimum drag coefficient with Reynolds number for trapezoid-wing configuration. $C_{L,design} = 0$; nacelles on.

19
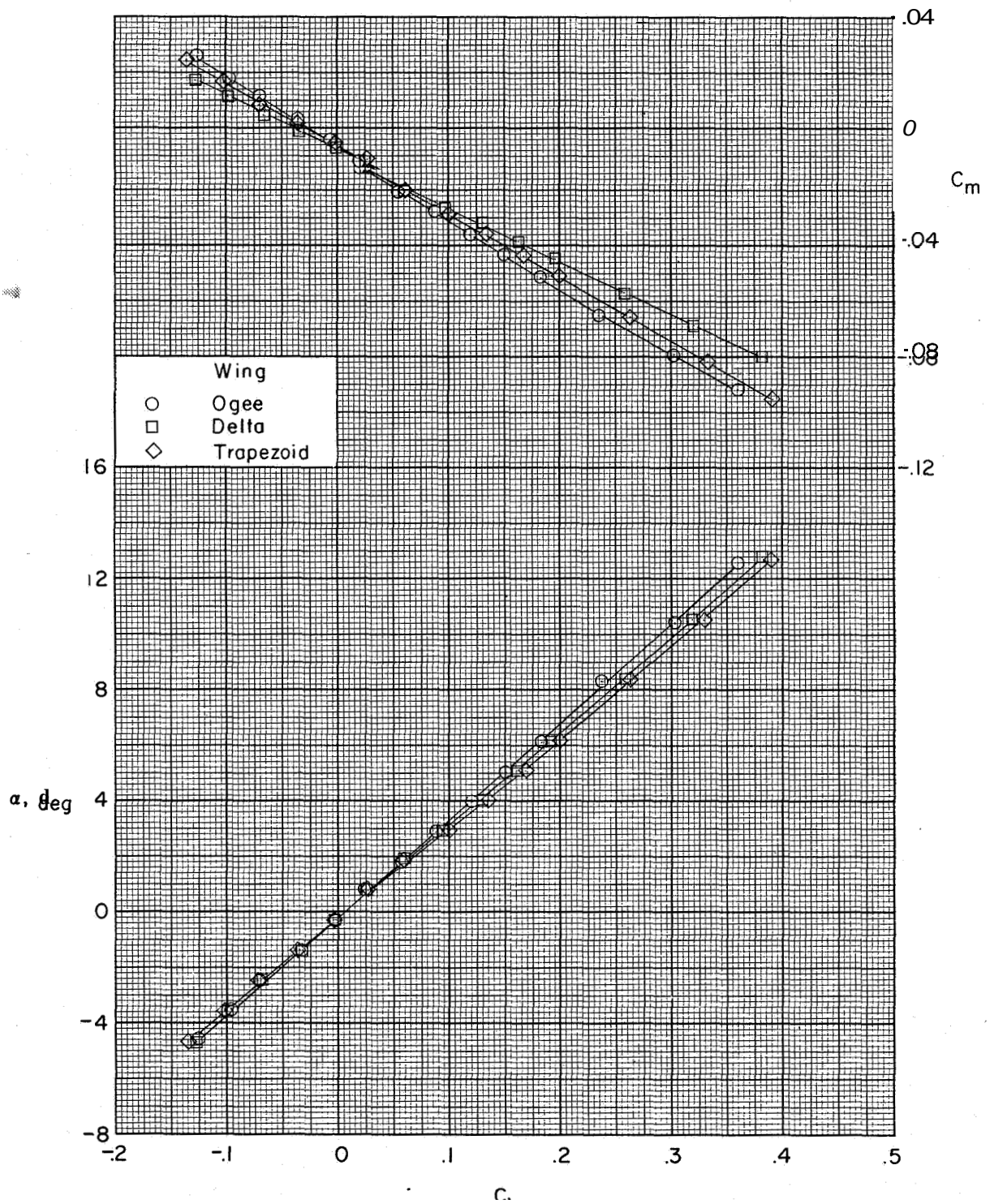
(a) Nacelles on.

Figure 7.- Effect of wing planform on the longitudinal characteristics. $C_{L,design} = 0$.
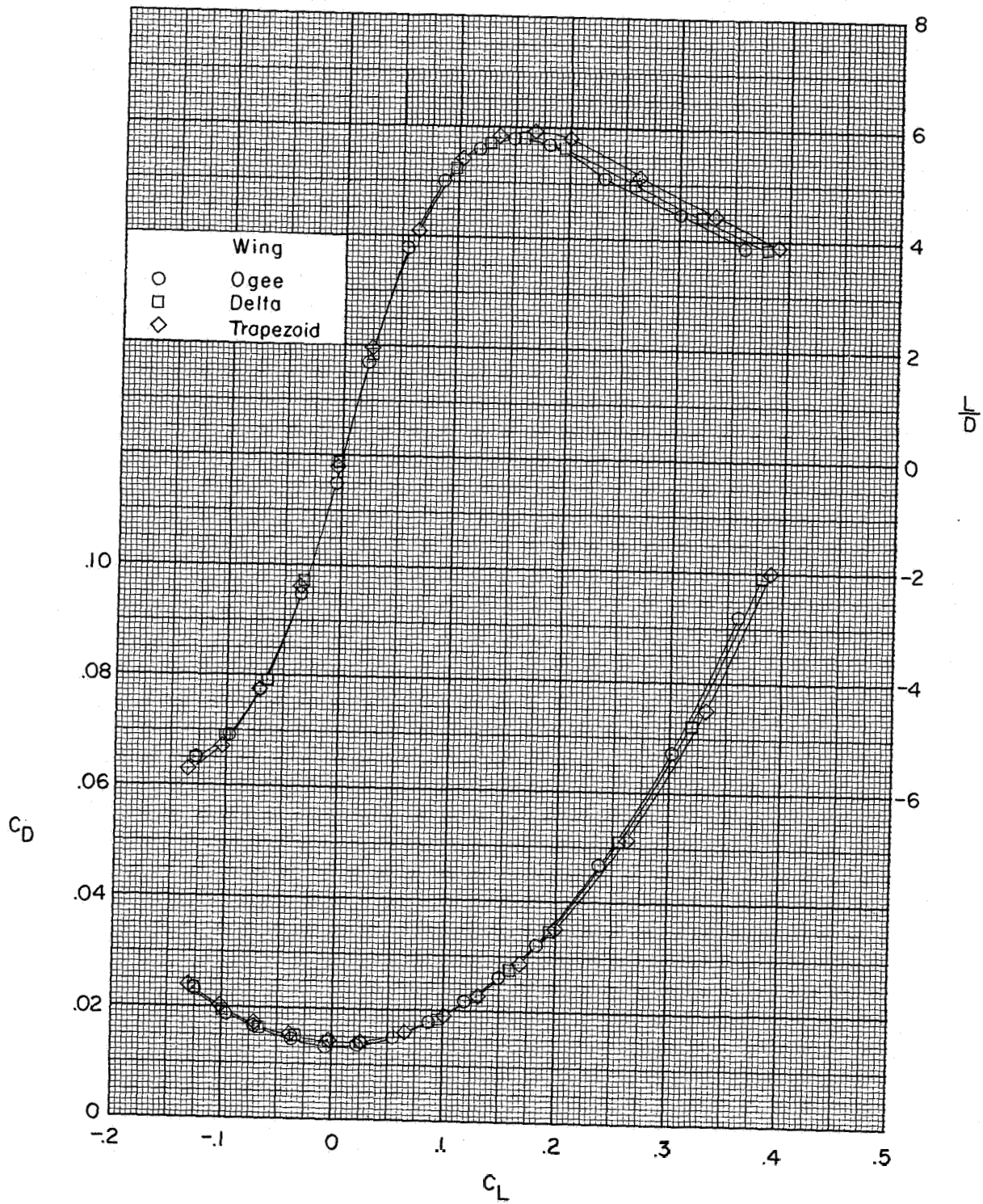
(a) Concluded.

Figure 7.- Continued.
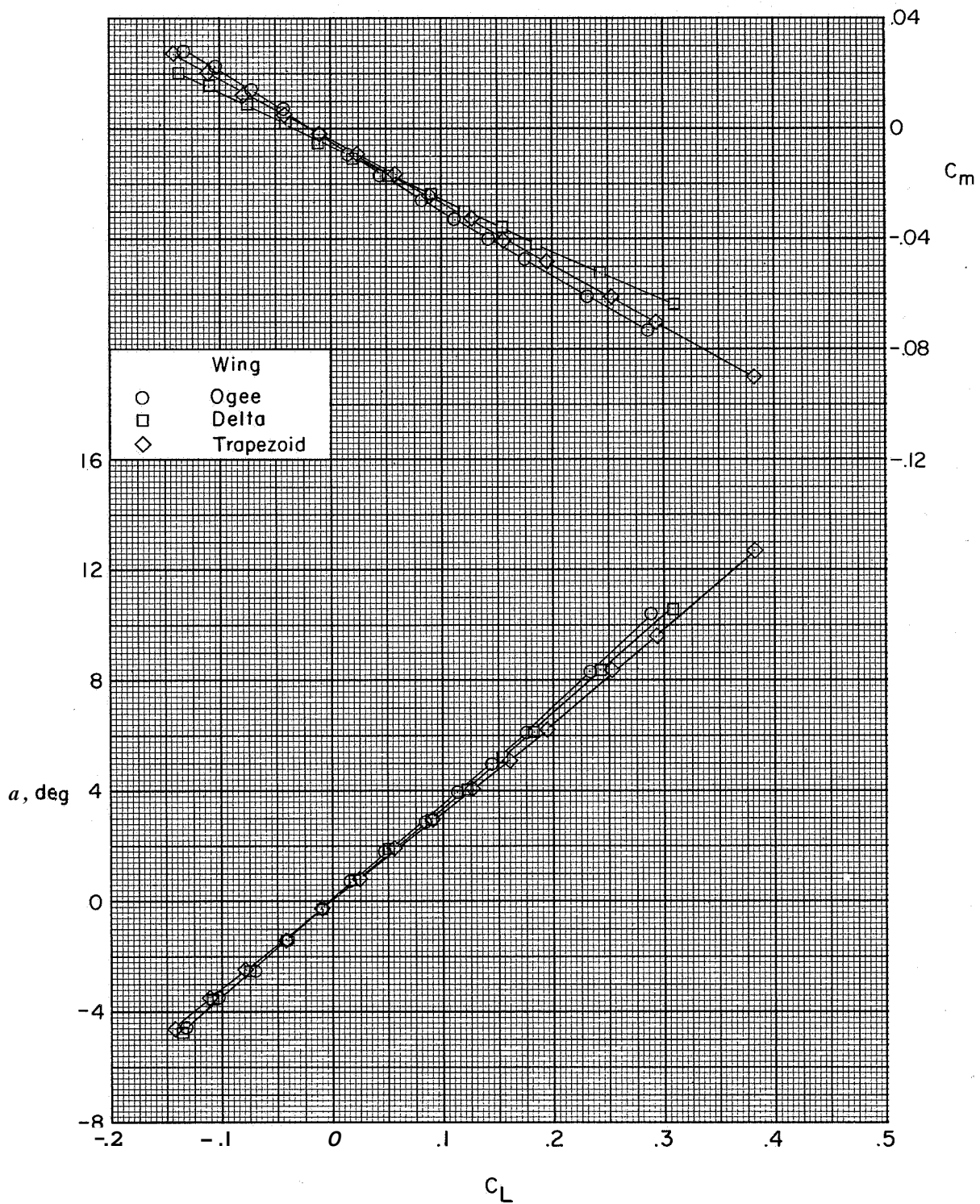
(b) Nacelles off.

Figure 7.- Continued.

(b) Concluded.
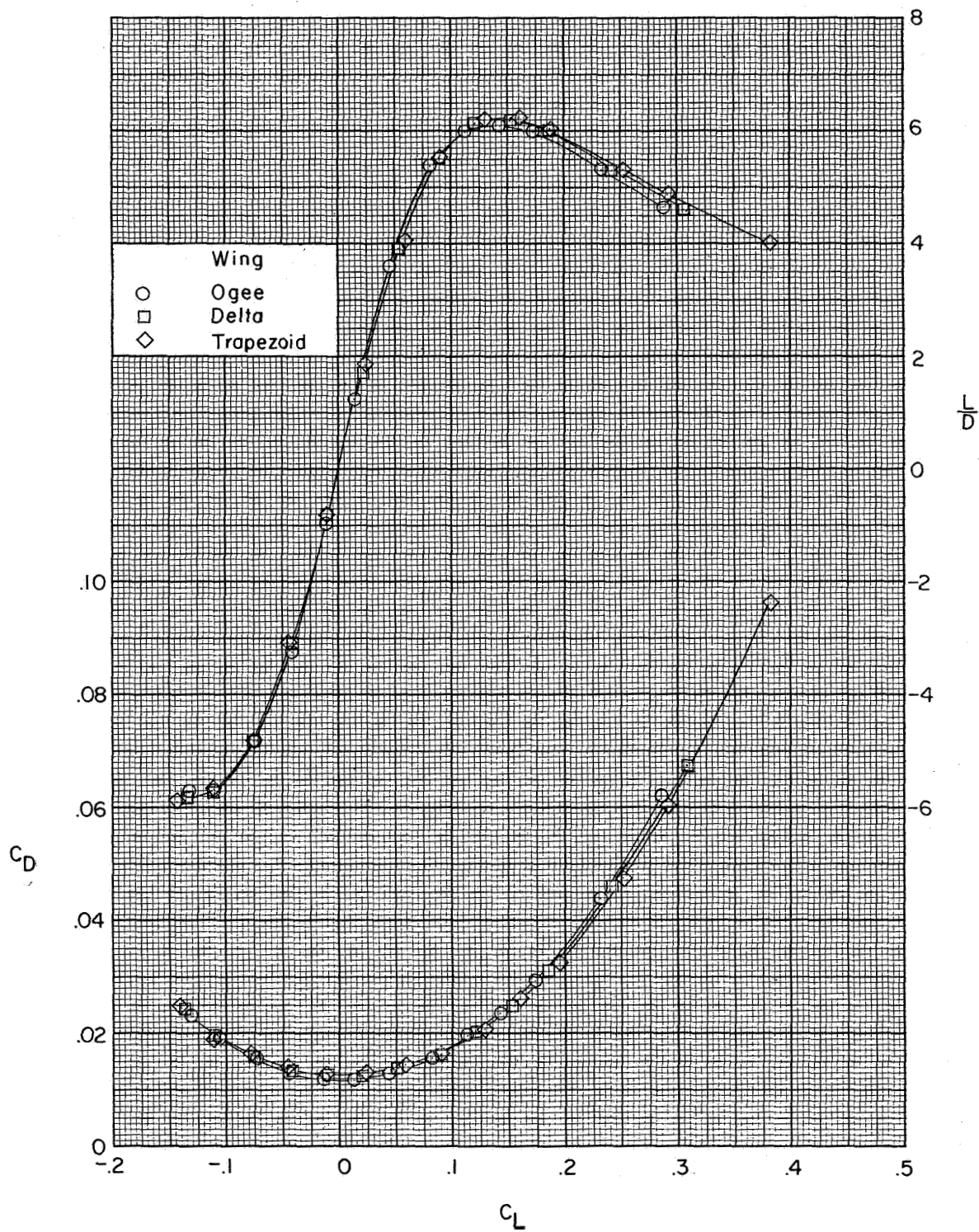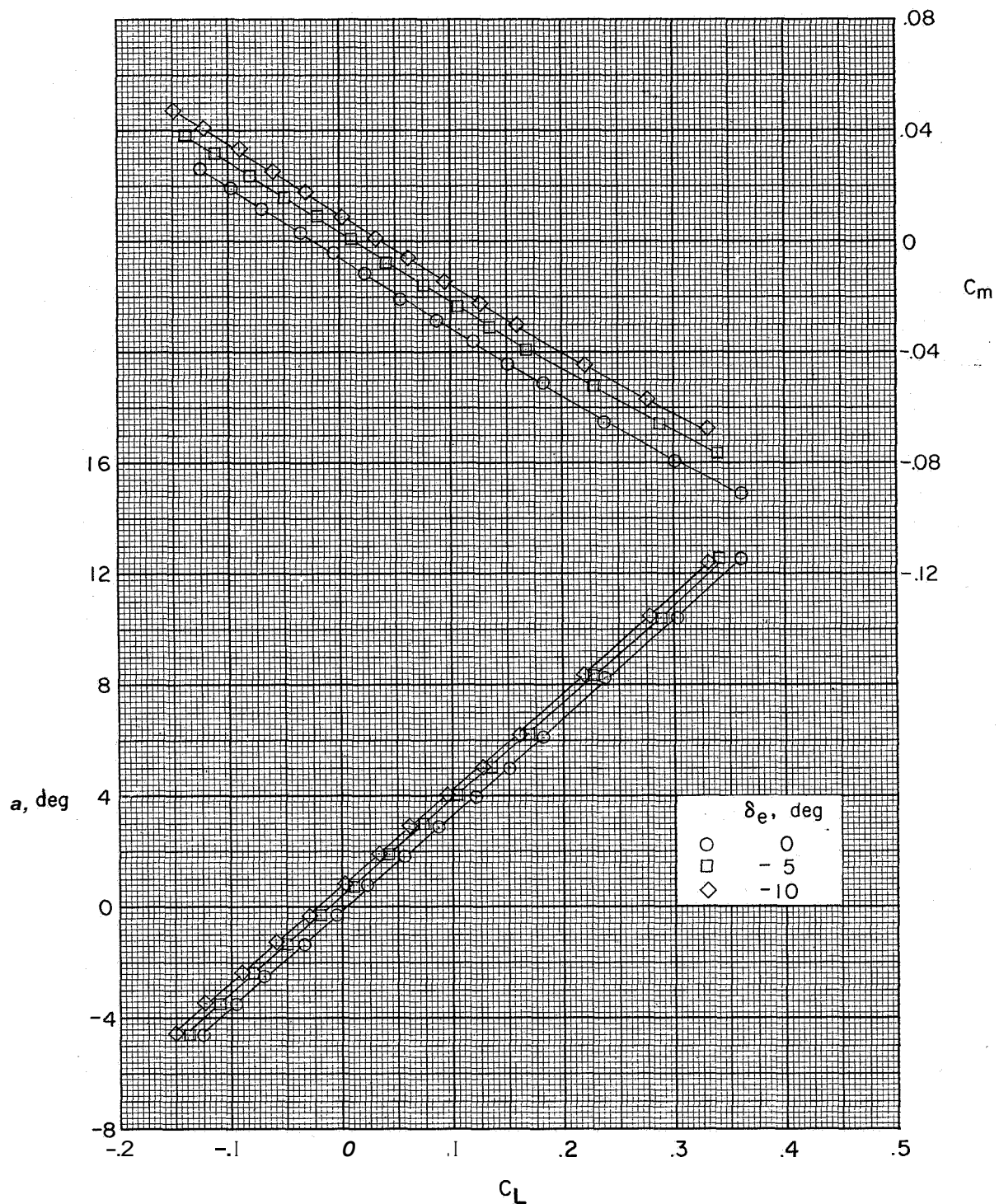
Figure 7.- Concluded.

(a) Ogee-wing configuration.

Figure 8.- Effect of elevon deflection on the longitudinal characteristics. $C_{L,design} = 0$; inboard and outboard controls deflected; nacelles on.
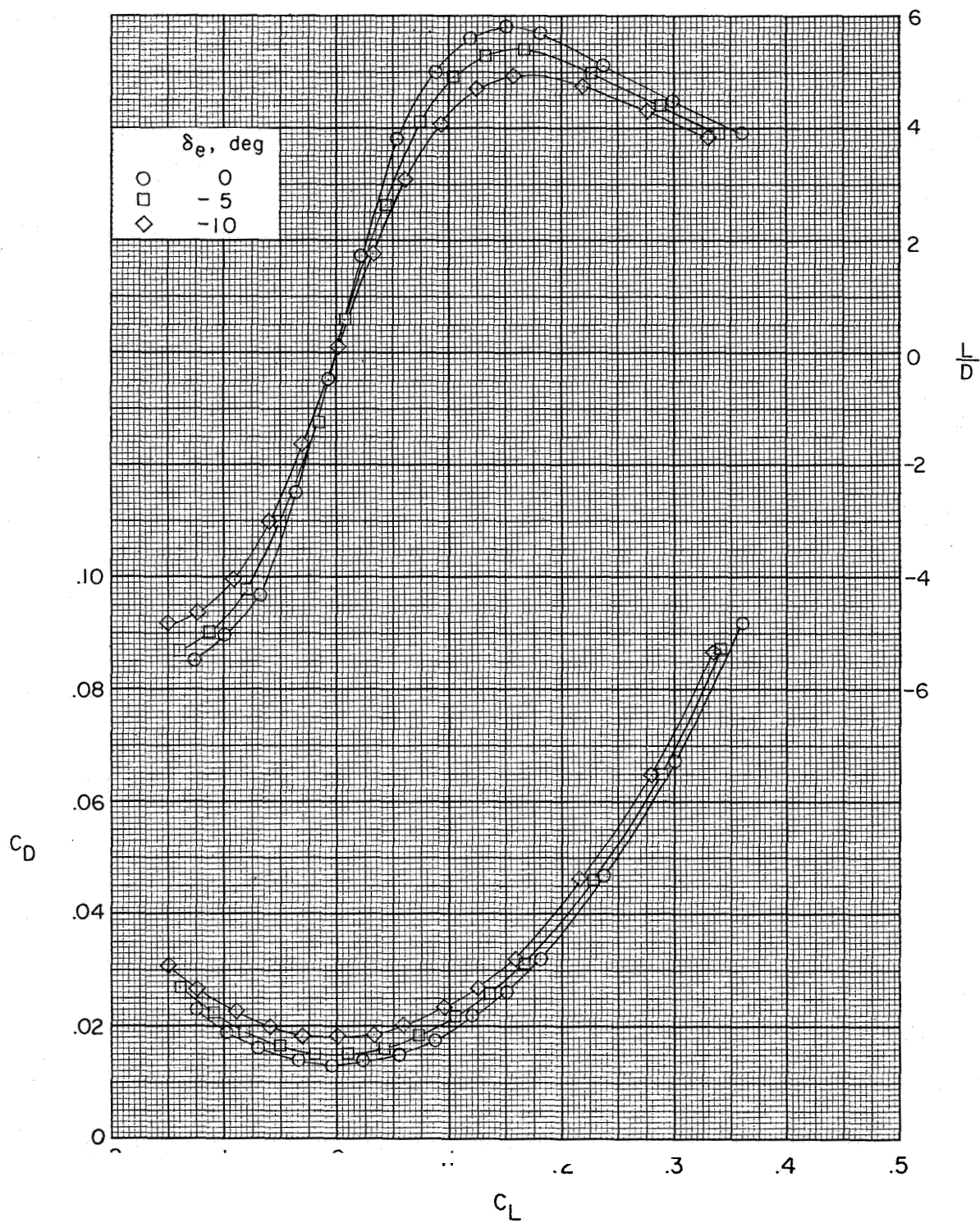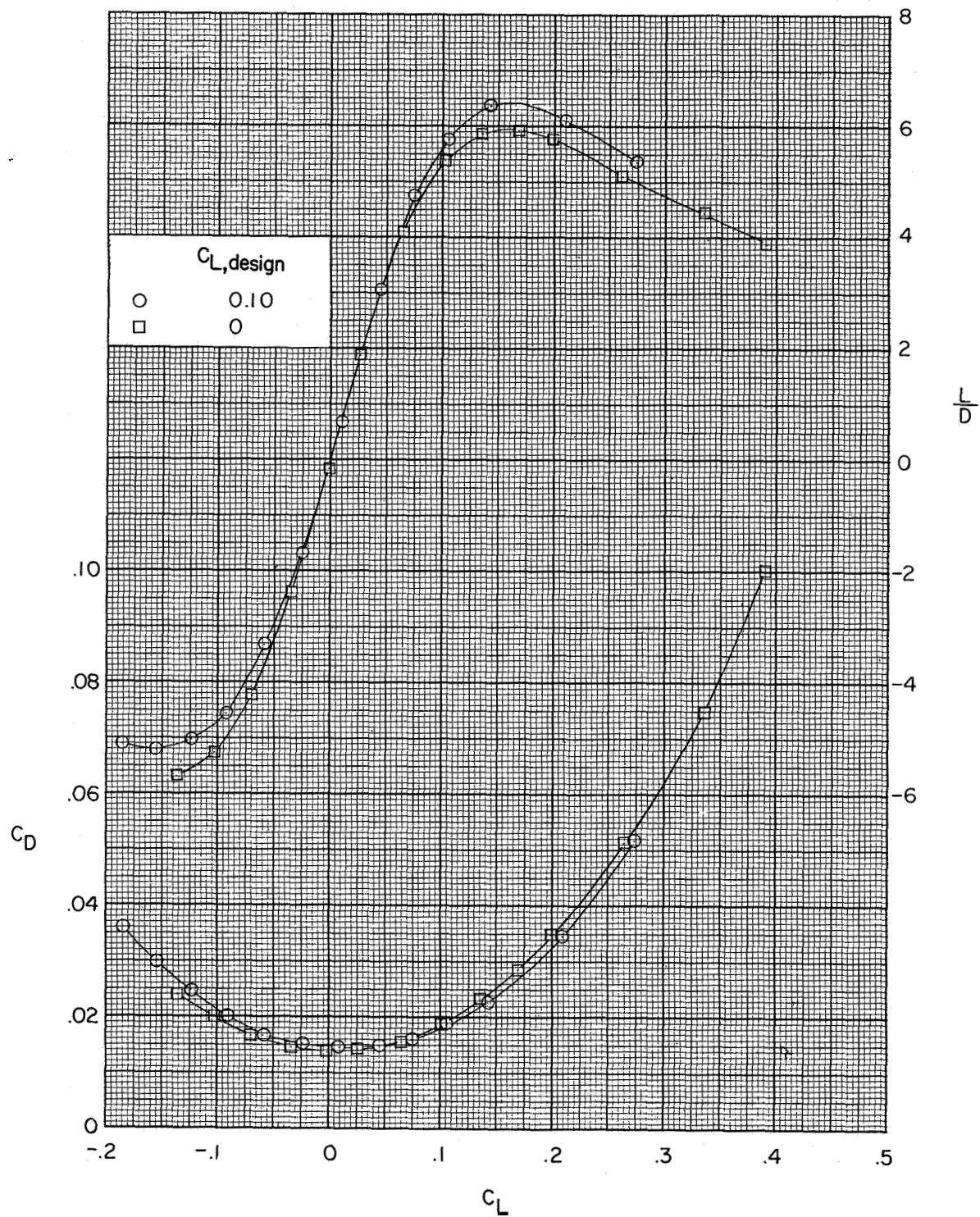
(a) Concluded.
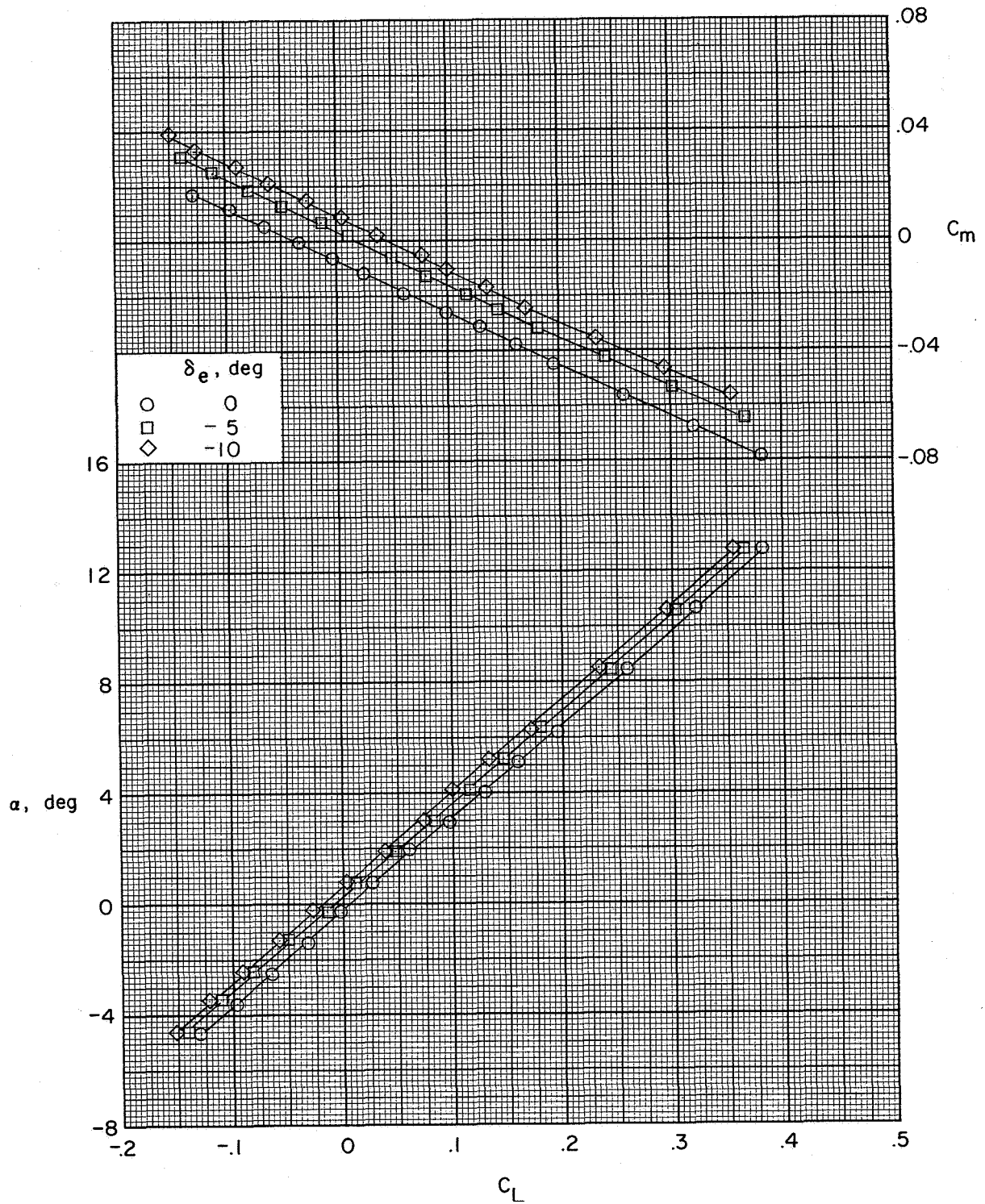
Figure 8.- Continued.

(b) Delta–wing configuration.
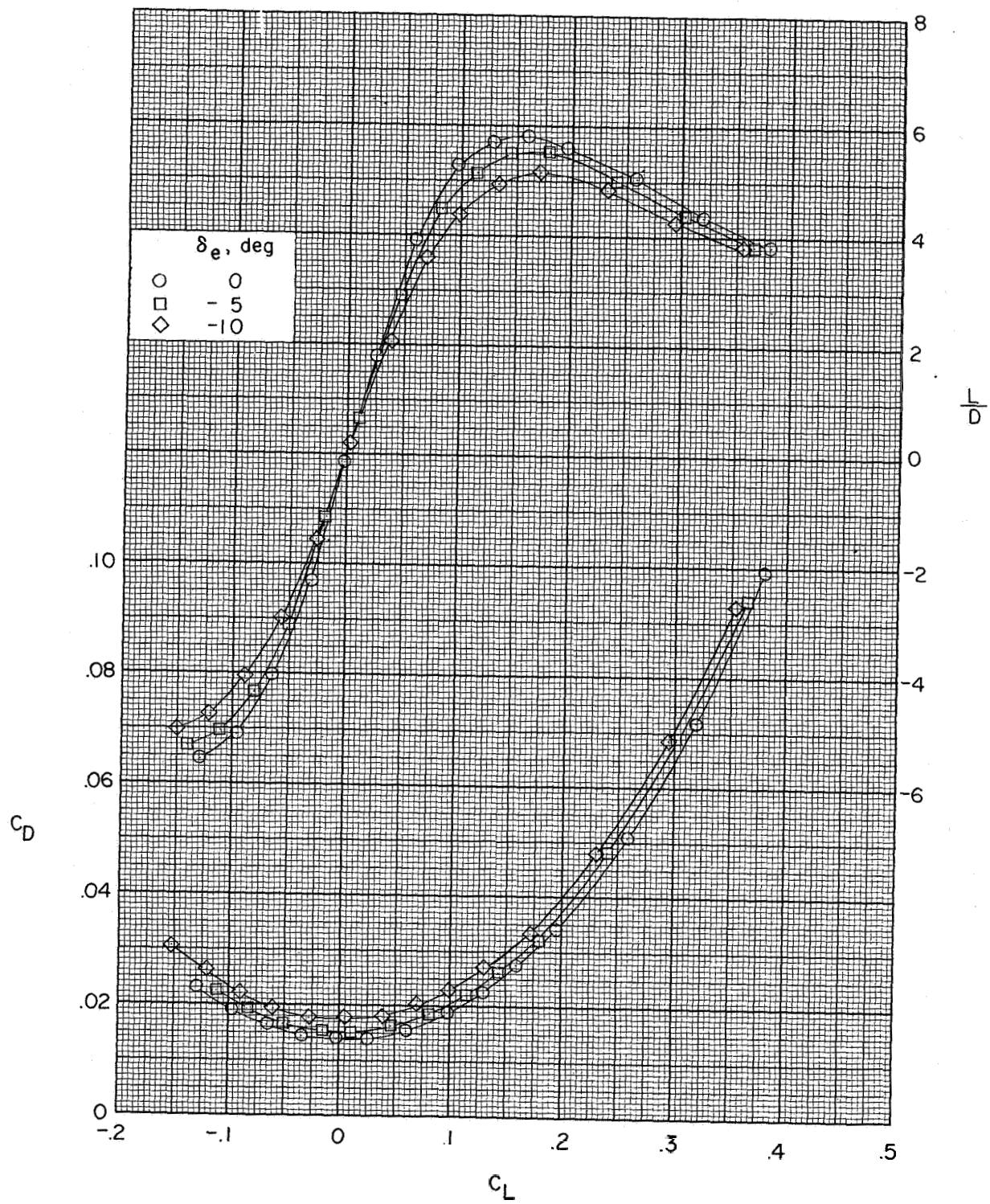
Figure 8.- Continued.

(b) Concluded.
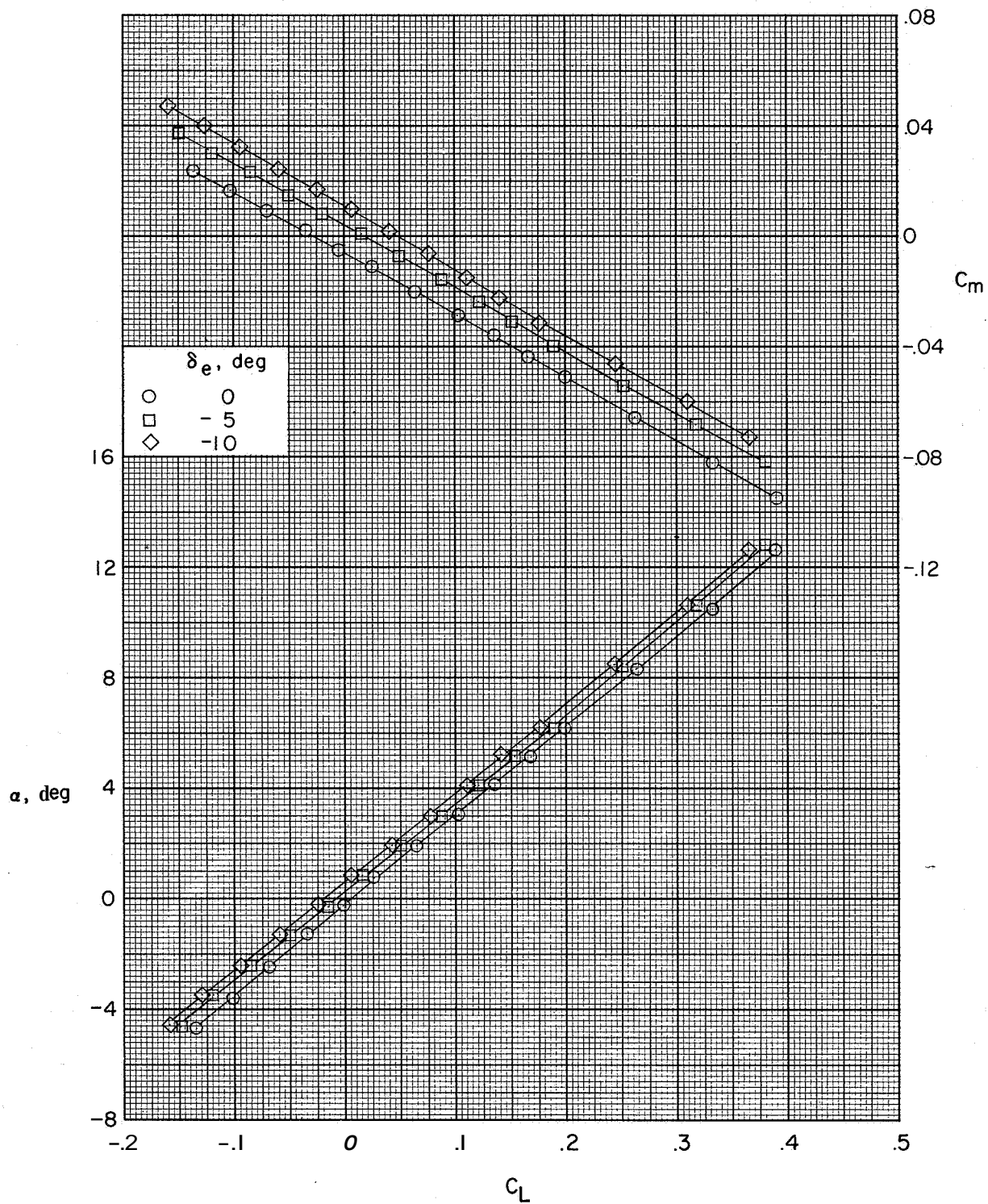
Figure 8.- Continued.

(c) Trapezoid-wing configuration,
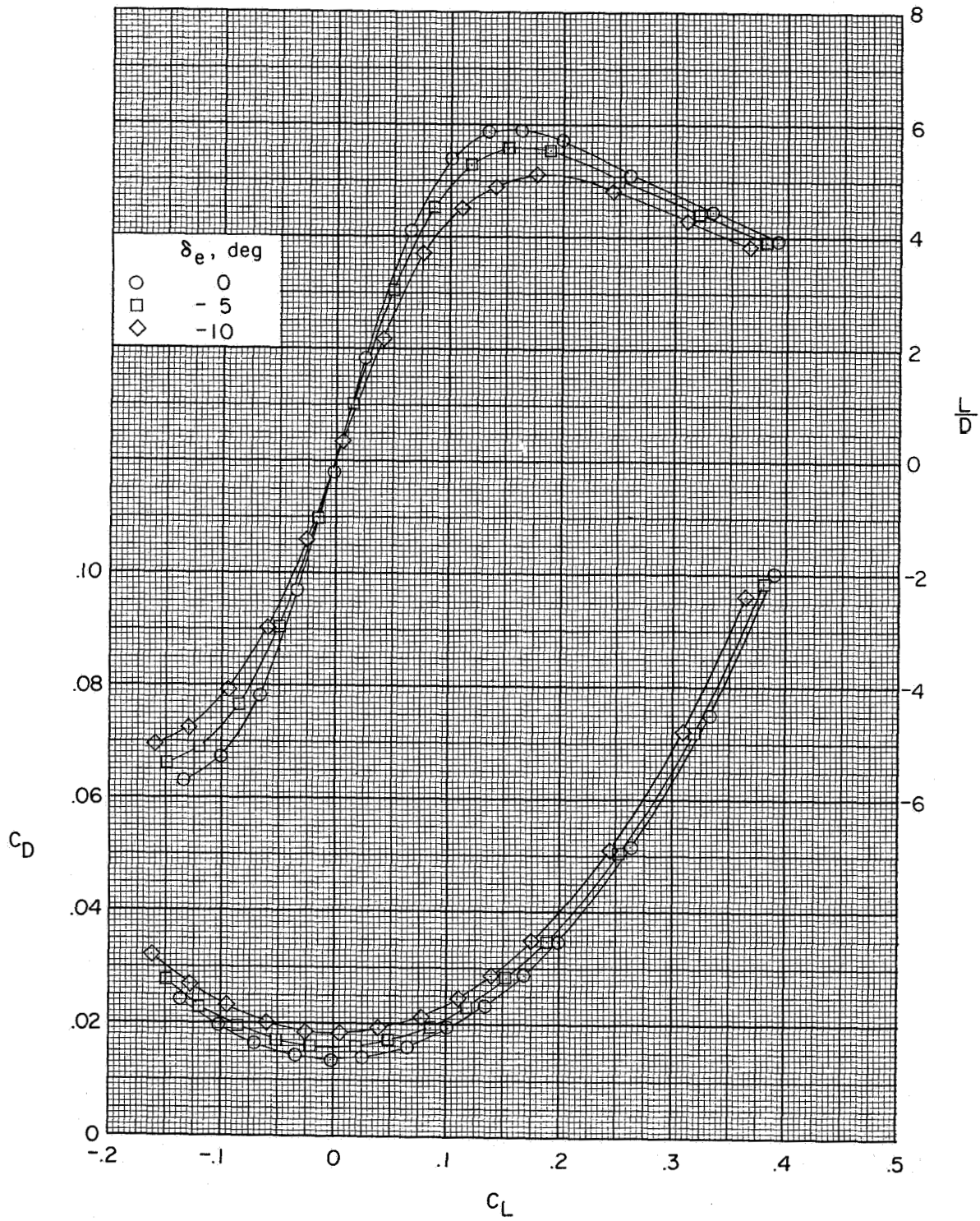
Figure 8.- Continued.

(c) Concluded.

Figure 8.- Concluded.
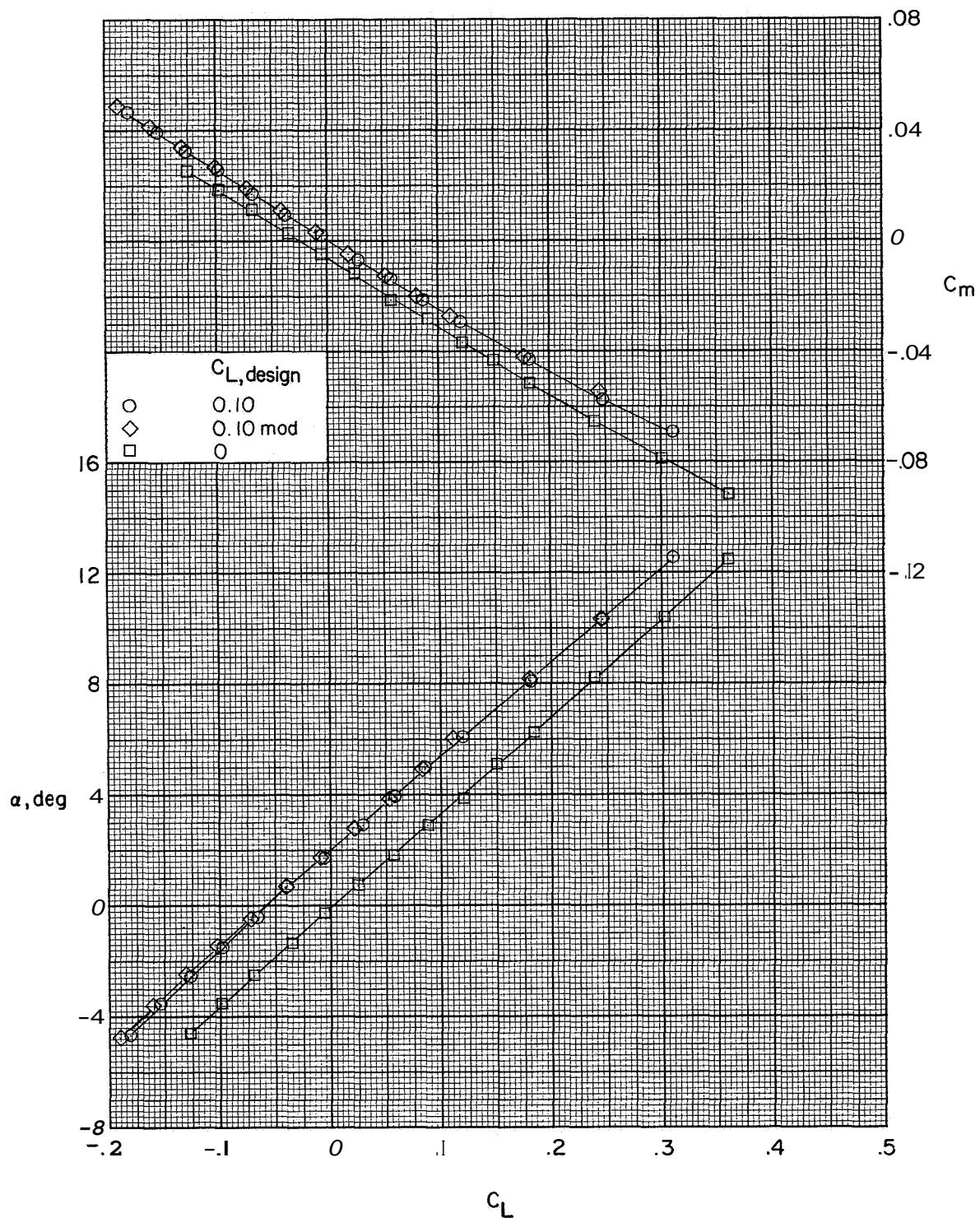
(a) Ogee-wing configuration.

Figure 9.- Effect of wing camber and twist on the longitudinal
characteristics. Nacelles on.
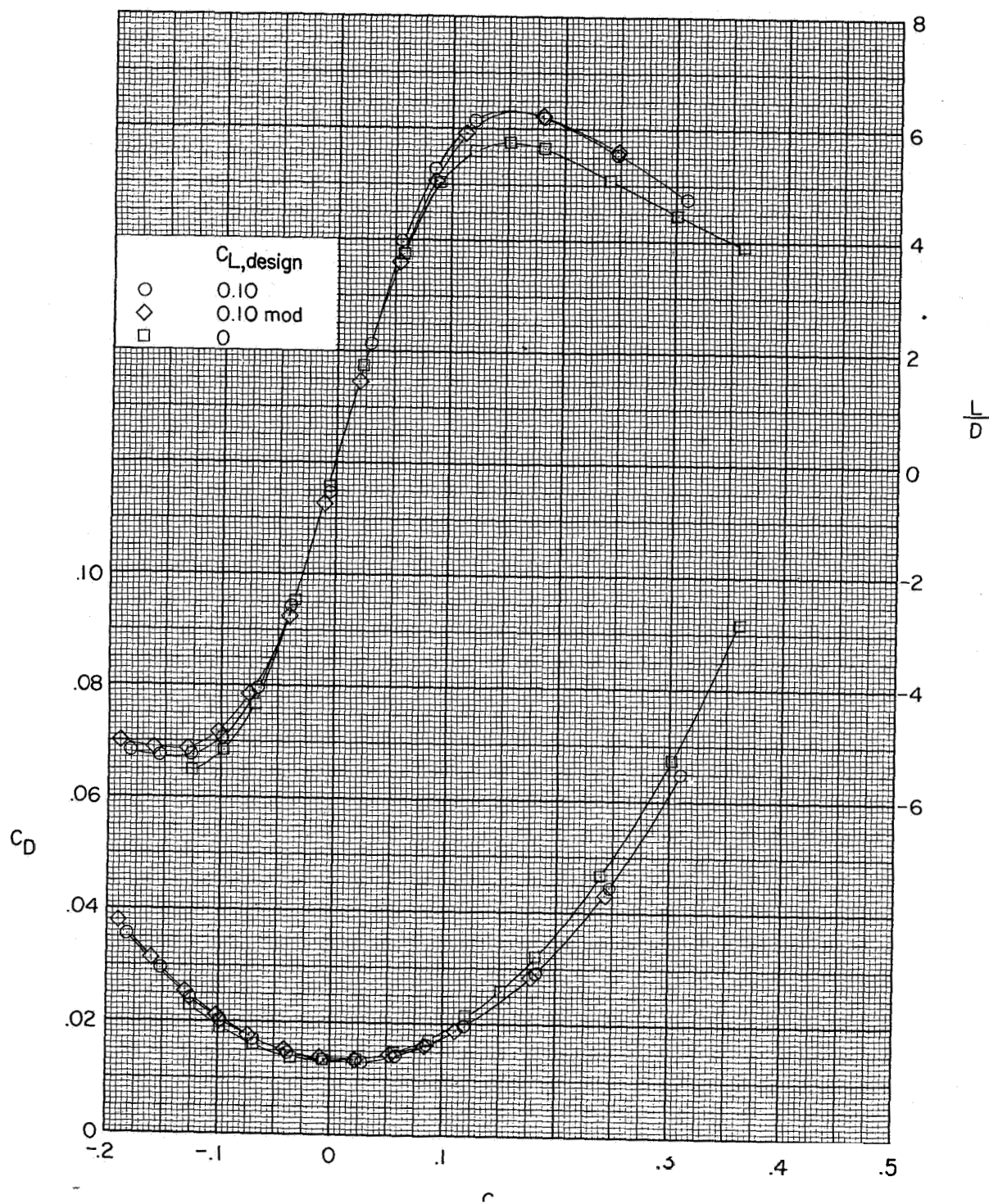
(a) Concluded,

Figure 9.- Continued.

(b) Delta-wing configuration.

Figure 9.- Continued.

Figure legend:

	$C_{L,design}$
○	0.10
□	0

C_D (vertical axis)

$\frac{L}{D}$ (right vertical axis)

C_L (horizontal axis)
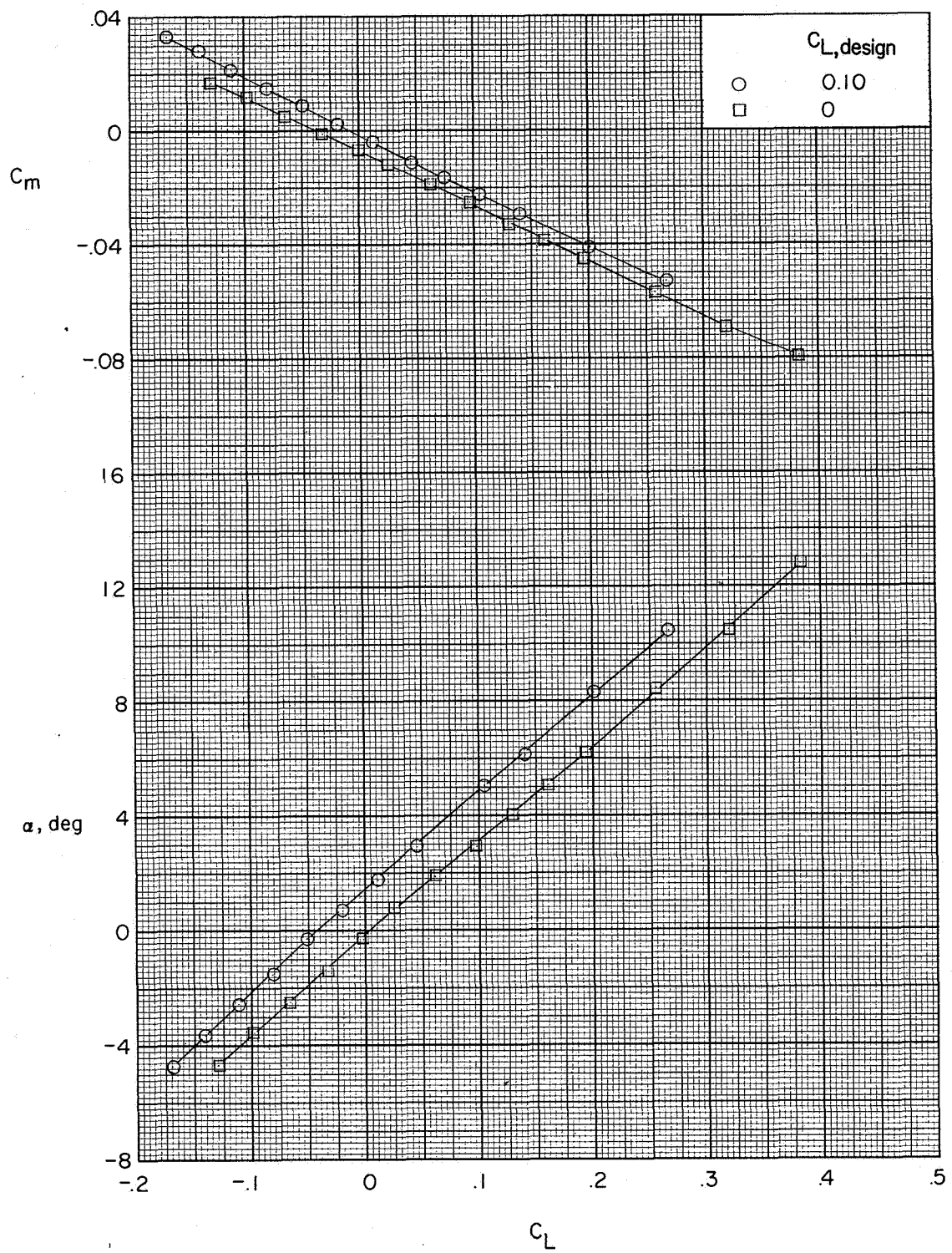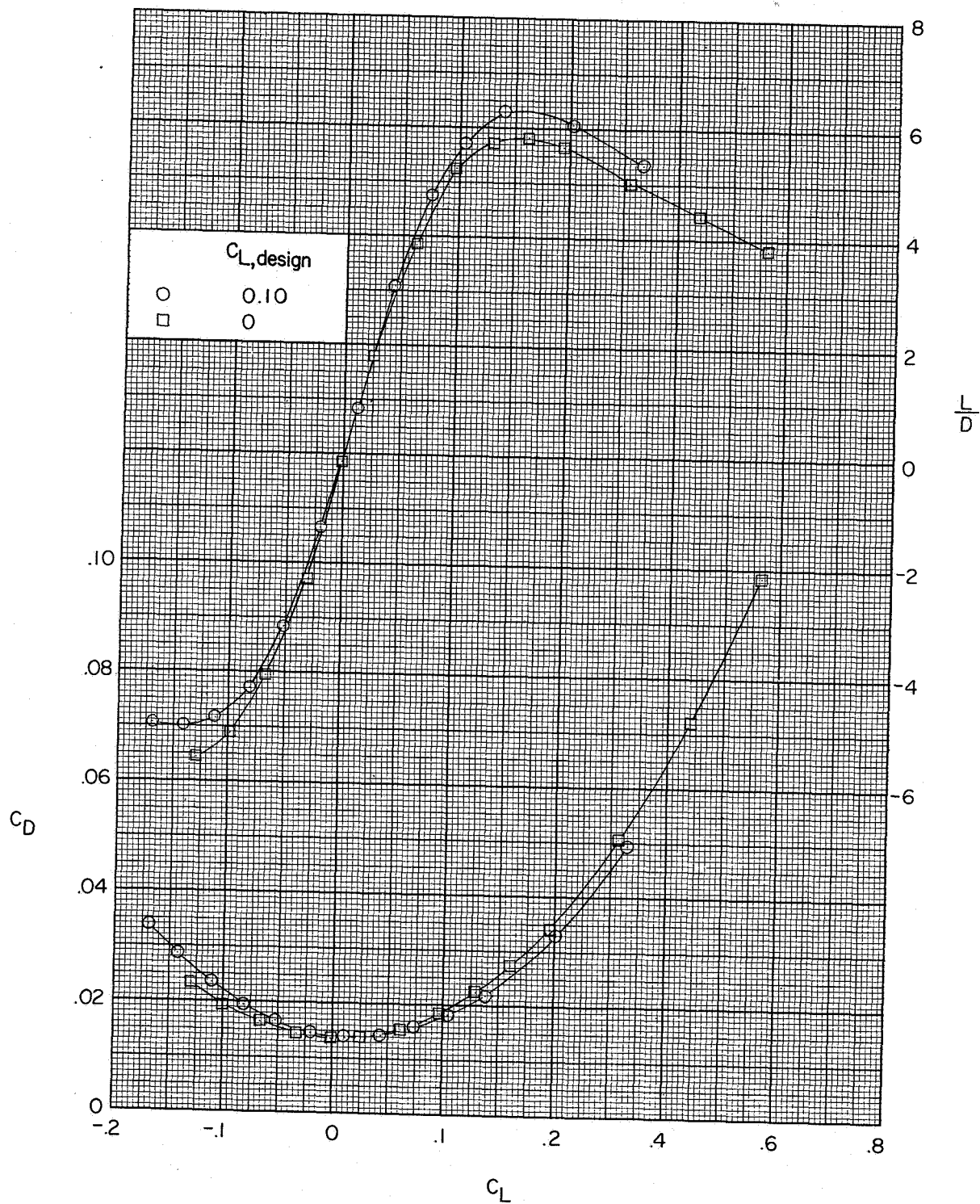
(b) Concluded.
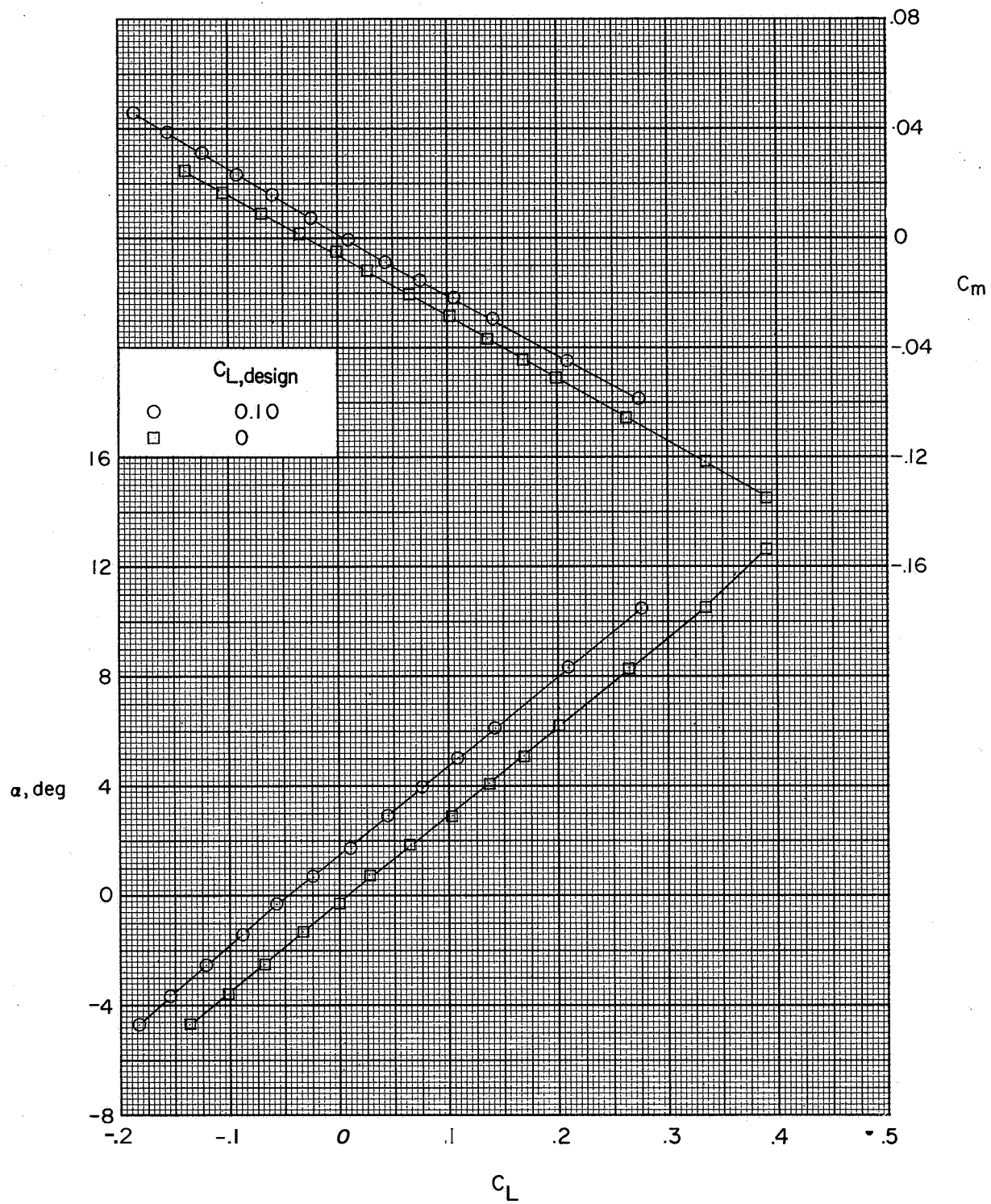
Figure 9.- Continued.

(c) Trapezoid-wing configuration.

Figure 9.- Continued.

(c) Concluded.

Figure 9.- Concluded.
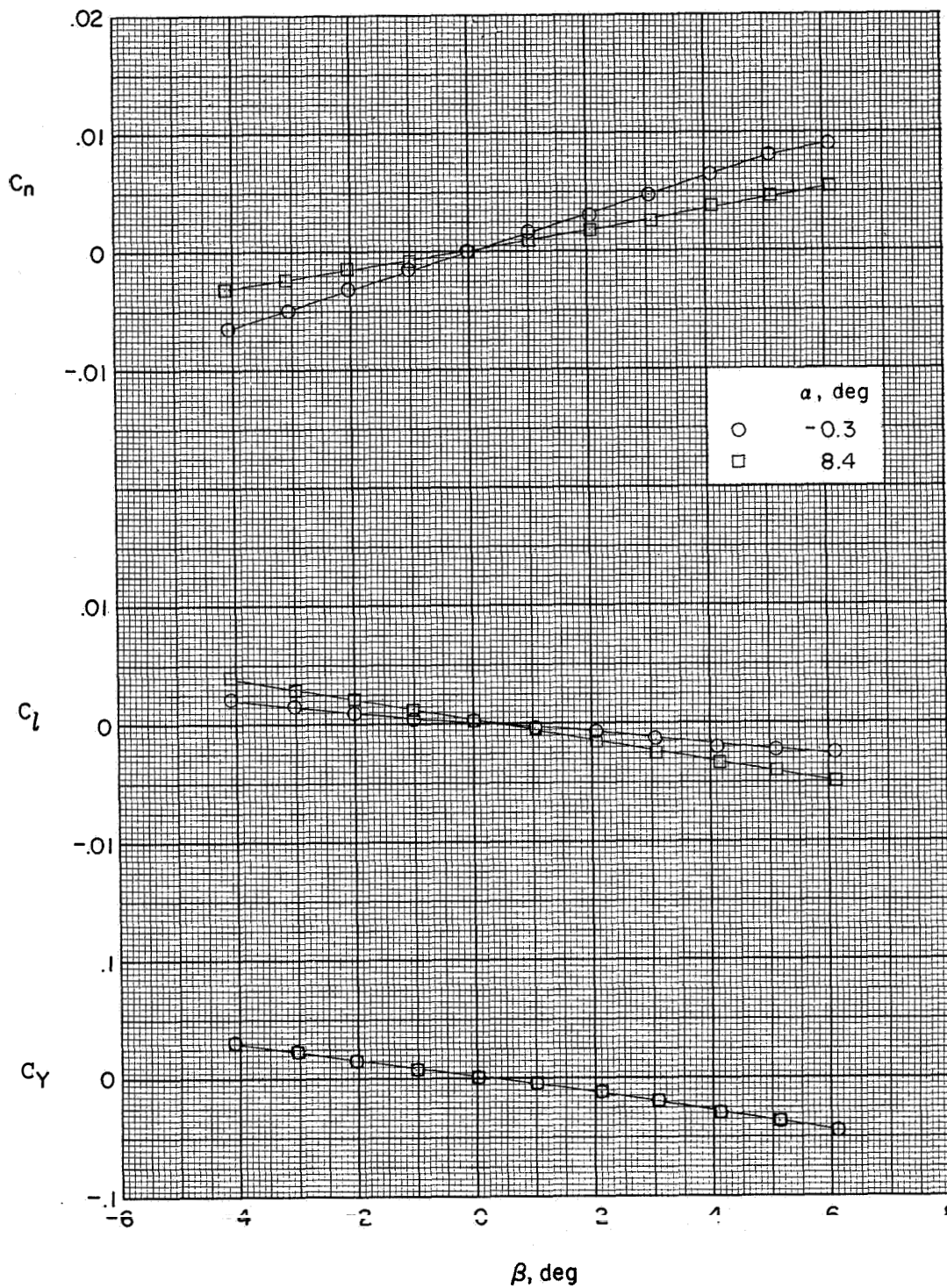
(a) Nacelles on.

Figure 10.- Aerodynamic characteristics of trapezoid-wing configuration in sideslip. $C_{L,design} = 0$.
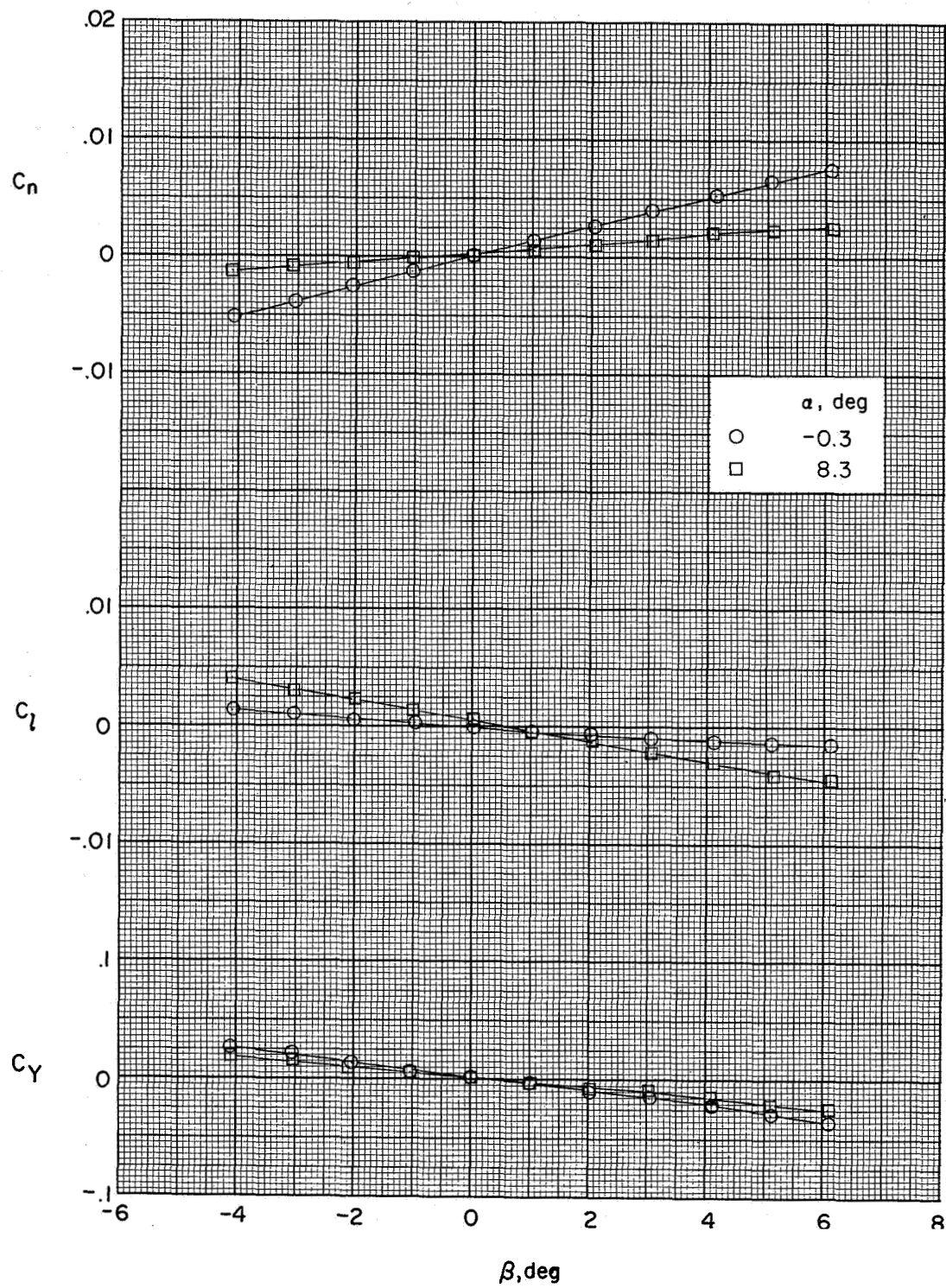
(b) Nacelles off.

Figure 10.- Concluded.
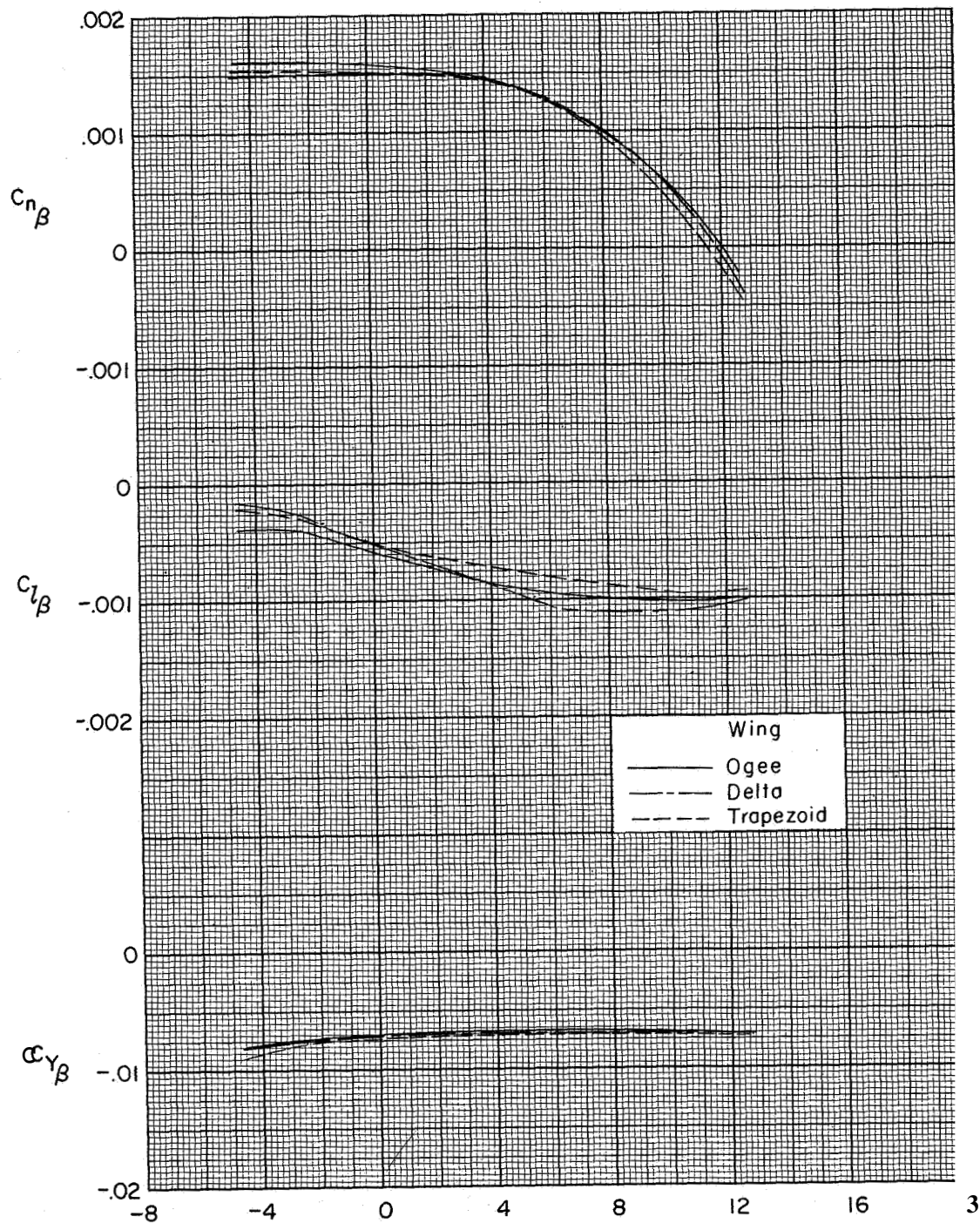
(a) $C_{L,design} = 0$.

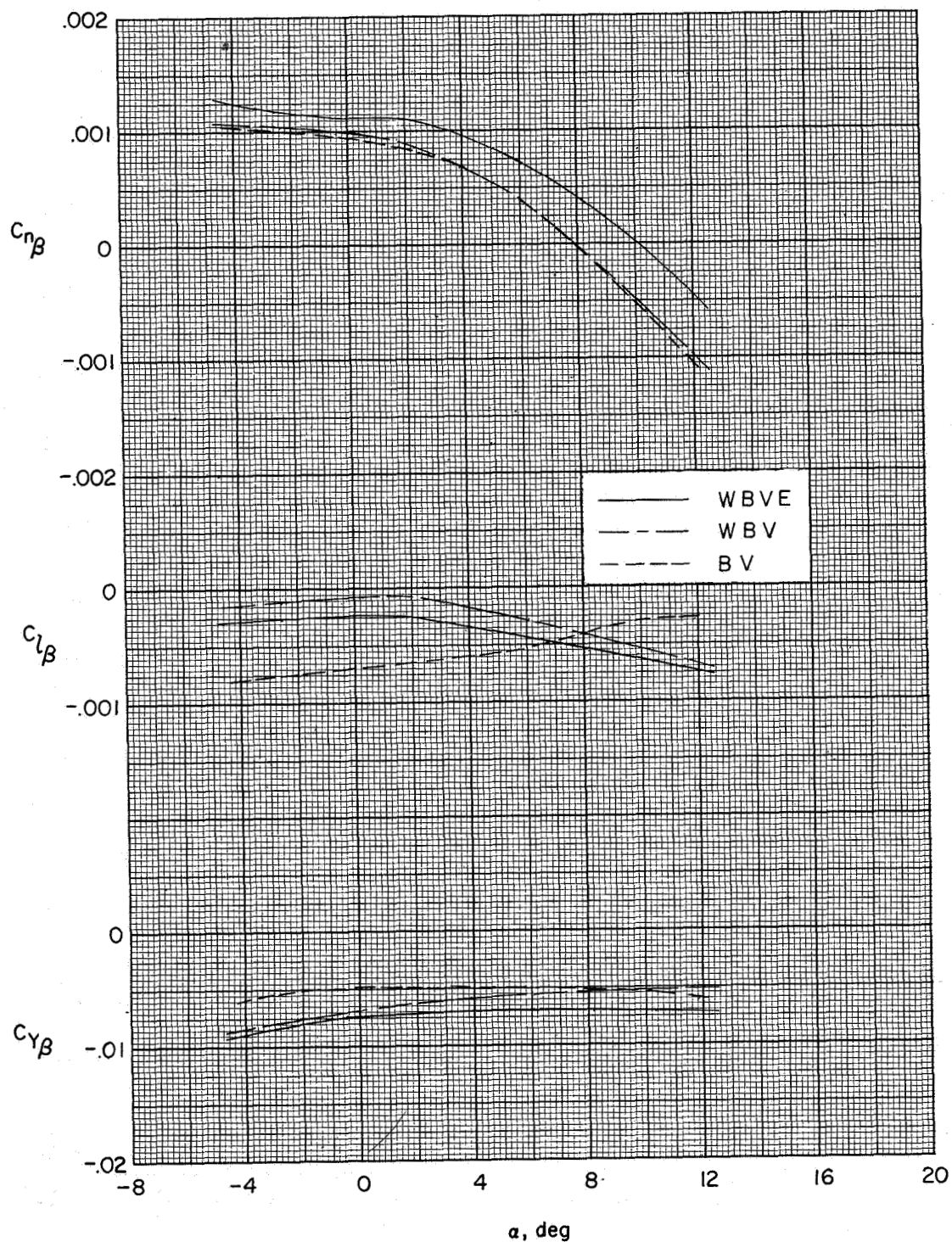Figure 11.- Effect of **wing planform** on the lateral and directional stability derivatives. Nacelles on.
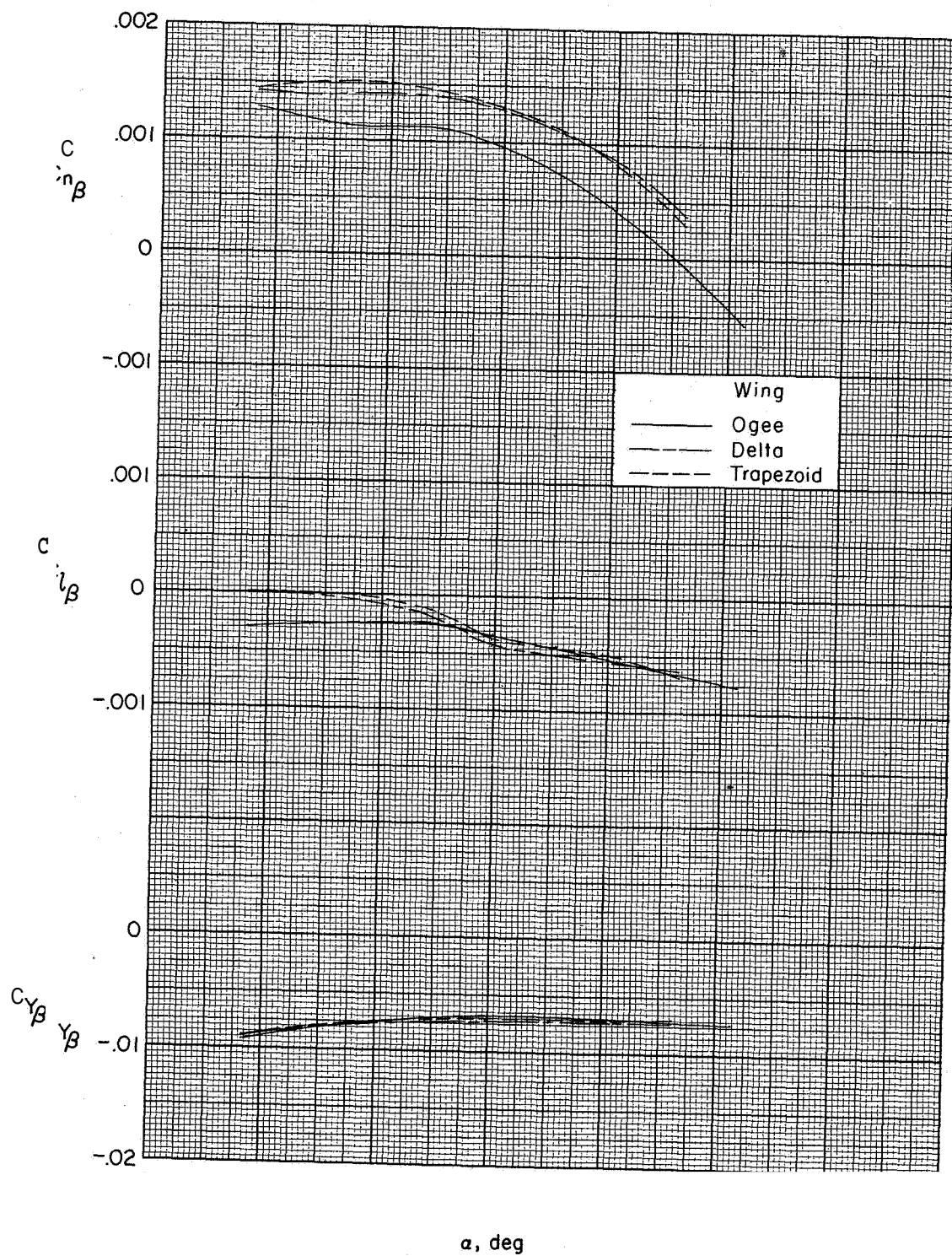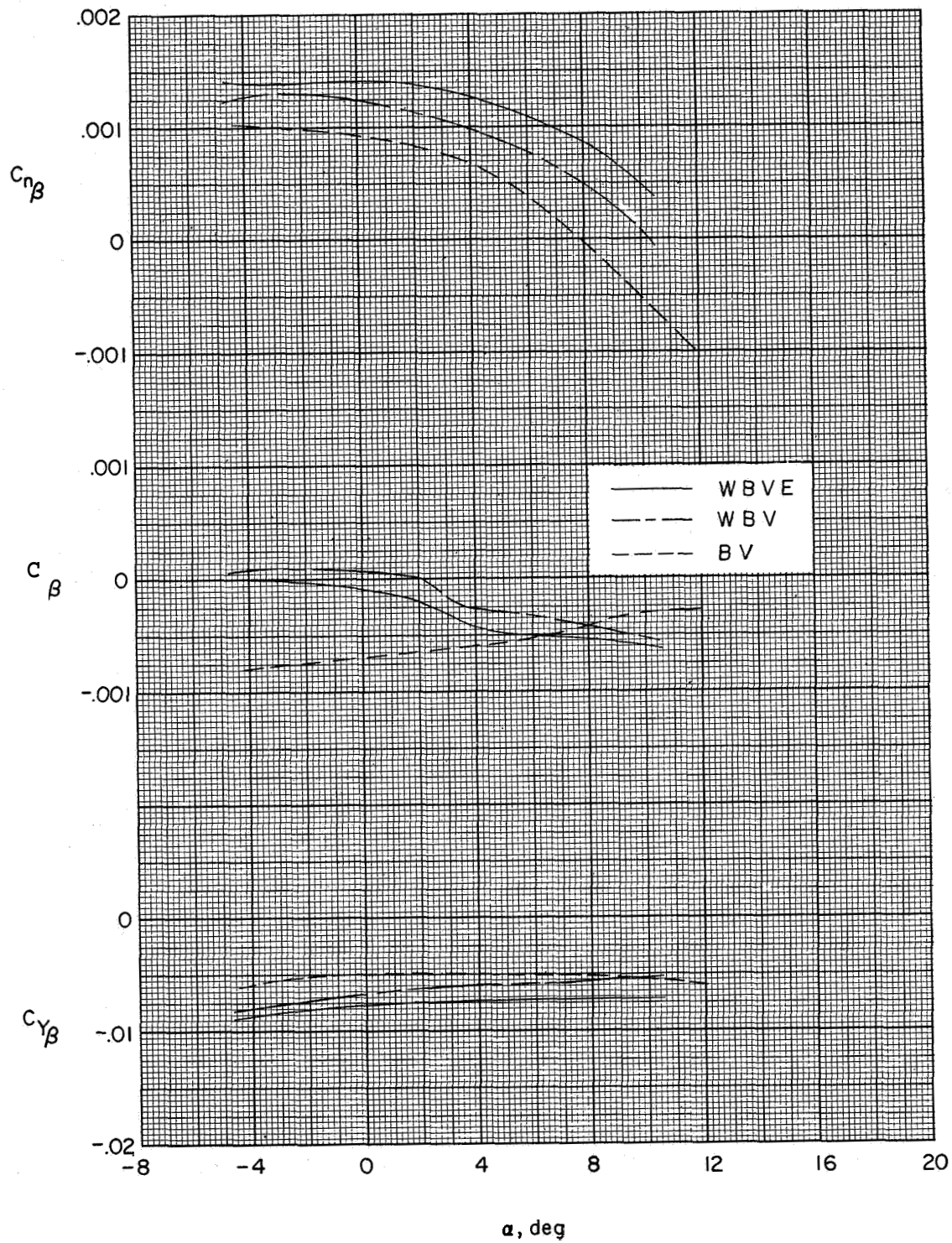
(b) $C_{L,design} = 0.1$.

Figure 11.- Concluded.
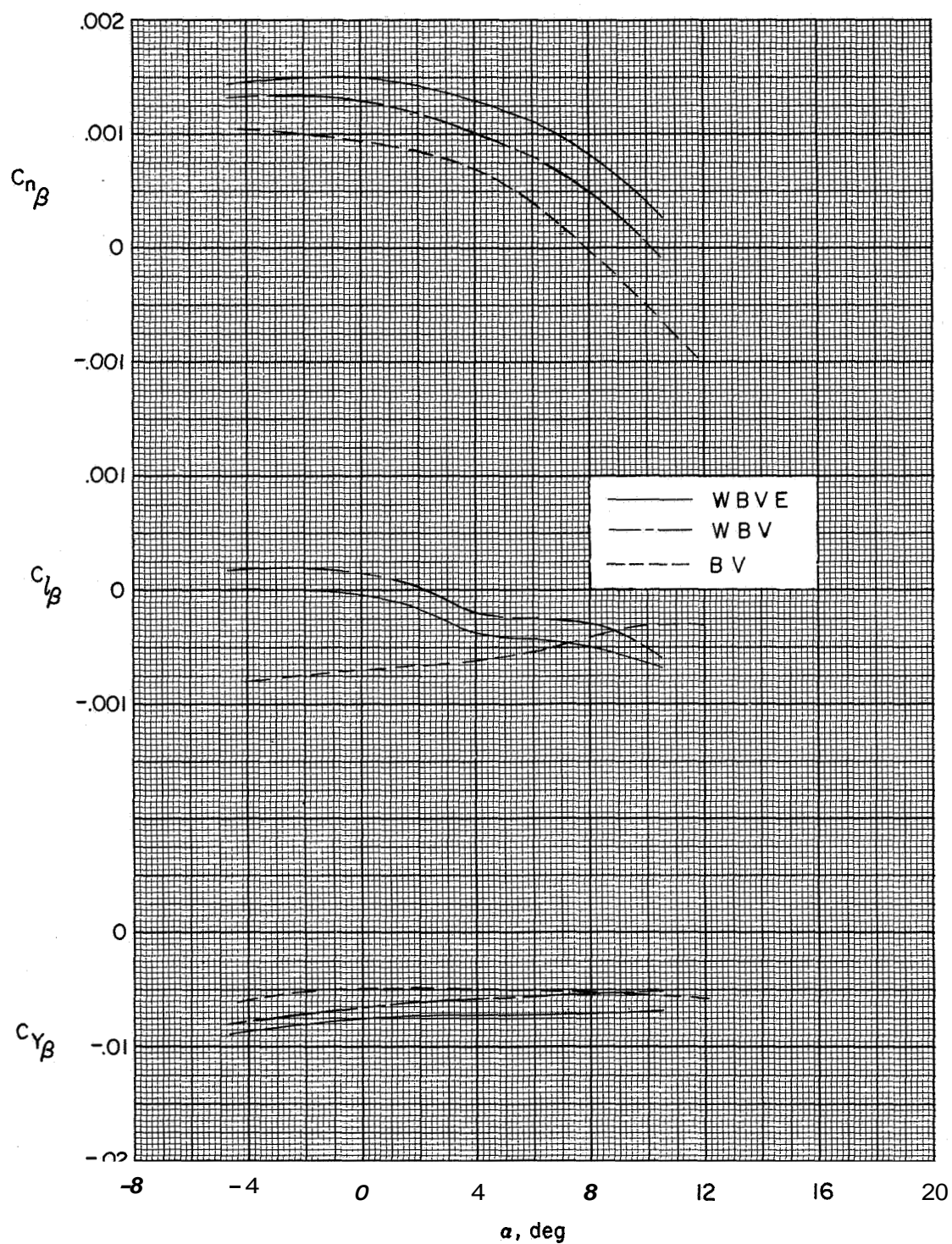
(a) Ogee-wing configuration.

Figure 12.- Effect of nacelles and wing on the lateral and directional stability derivatives. $C_{L,design} = 0.1$.

(b) Delta-wing configuration.

Figure 12.- Continued.

(c) Trapezoid-wing configuration.
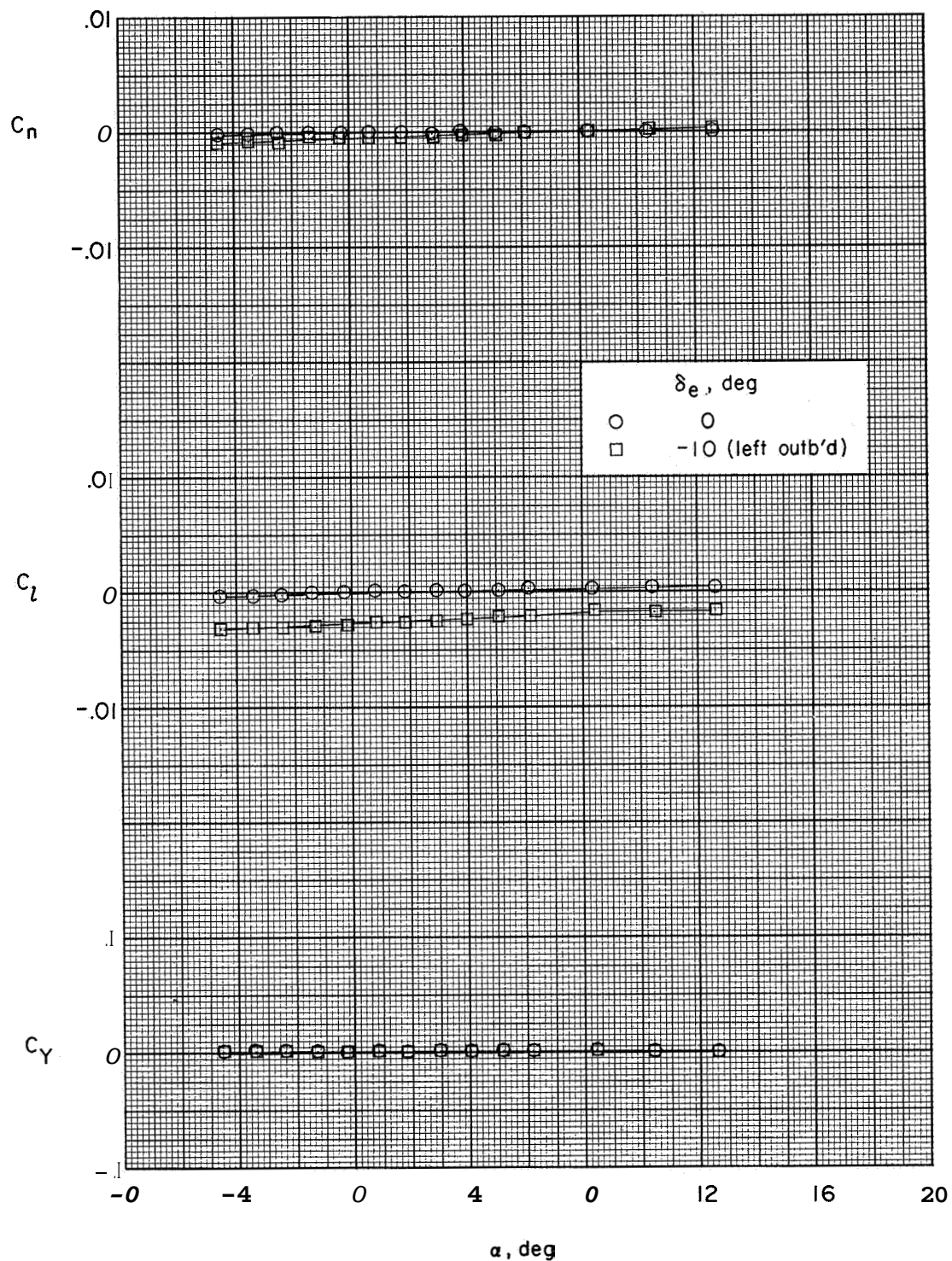
Figure 12.- Concluded.

Figure 13.- Roll control characteristics of outboard elevon on the ogee configuration. $C_{L,design} = 0$; nacelles on.